Climate Dynamics (2019) 52:6441–6461
https://doi.org/10.1007/s00382-018-4522-7

West African Monsoon: current state and future projections in a high-resolution AGCM

Jerry Raj[1] · **Hamza Kunhu Bangalath**[1] · **Georgiy Stenchikov**[1]

Received: 25 December 2017 / Accepted: 29 October 2018 / Published online: 2 November 2018

Abstract
The West African Monsoon (WAM) involves the interaction of multi-scale processes ranging from planetary to cumulus scales, which makes it challenging for coarse resolution General Circulation Models to accurately simulate WAM. The present study evaluates the ability of the high-resolution (~ 25 km) Atmospheric General Circulation Model HiRAM to simulate the WAM and to analyze its future projections by the end of the 21st century. For the historical period, two AMIP-type simulations were conducted, one forced with observed SST from Hadley Center Sea Ice and Sea Surface Temperature dataset and the other forced with SST from the coarse resolution Earth System Model (ESM2M), which is the parent model of HiRAM, i.e. both models have the same dynamical core and similar physical parameterizations. The future projection, using the Representative Concentration Pathway 8.5 and SST from ESM2M is also conducted. A process-based evaluation is carried out to elucidate HiRAM's ability to represent the key processes and multiscale dynamic features those define the WAM circulation. Compared to ESM2M, HiRAM better represents most of the key circulation elements at different scales, and thus more accurately represents the intensity and spatial distribution of the WAM rainfall. The position of the African easterly jet is considerably improved in HiRAM simulations, leading to the improved positioning of the WAM rainbelt and the two-cell structure of convection. The future projection of the WAM exhibits warming over the entire domain, decreasing precipitation over the southern Sahel, and increase of precipitation over the western Sahara.

Keywords West African Monsoon · High-resolution AGCM · GFDL HiRAM

1 Introduction

West Africa, the home for more than 300 million people, is one of the most vulnerable regions to global warming due to its high exposure and low adaptive capacity (Barros et al. 2015). The agriculture-based economy of the region highly relies on the West African Monsoon (WAM), which produces a mean annual rainfall of 150–2500 mm. The variability and change of WAM can have a devastating impact on the local population, especially since the region lacks sufficient irrigation infrastructure (Boko et al. 2007). Furthermore, the region is infamous for its climate extremes (Nicholson 2013), which cause extensive socioeconomic impacts (Cornforth 2012). Therefore, the accurate simulation, and projection of the WAM are of utmost importance for improving the adaptability of the region. However, according to IPCC AR5, there is "low to medium confidence" in the robustness of projected rainfall change over West Africa due to the considerable inter-model variations in both the magnitude and the sign of change. This disparity can be partially attributed to the inability of conventional general circulation models (GCMs) to resolve the convective rainfall (Stocker et al. 2013). The present study thus serves as an effort to explore the effect of finer spatial resolution on the current state and future projection of the WAM.

In recent years, simulation of West African climate has received much attention and generated a series of research initiatives to comparatively assess the modeling of WAM, e.g., African Multidisciplinary Monsoon Analysis Model Intercomparison Project (AMMA-MIP) (Hourdin et al.

✉ Jerry Raj
jerry.raj@kaust.edu.sa

Hamza Kunhu Bangalath
hamzakunhu.bangalath@kaust.edu.sa

Georgiy Stenchikov
georgiy.stenchikov@kaust.edu.sa

[1] Physical Science and Engineering Division (PSE), King Abdullah University of Science and Technology (KAUST), Thuwal 23955-6900, Saudi Arabia

2010), the AMMA Land-surface Model Intercomparison Project (ALMIP) (Boone et al. 2009), the West African Monsoon Modeling and Evaluation (WAMME) project (Xue et al. 2010; Druyan et al. 2010), the Ensembles-Based Predictions of Climate Change and their Impacts (ENSEMBLES) African project (Paeth et al. 2011), and the Coordinated Regional Downscaling Experiment (CORDEX) (Jones et al. 2011; Giorgi et al. 2009). However, the majority of the models involved in these projects are either coarse resolution GCMs or regional climate models (RCMs). Simulations of WAM using GCMs often suffer from shortcomings associated with their coarse spatial resolution (Hourdin et al. 2010; Sylla et al. 2010; Xue et al. 2010). This limitation of coarse resolution GCMs is partly due to the poorly resolved effects of vegetation, orography, and coastlines, which are important controls on the regional precipitation pattern. Furthermore, coarser resolution GCMs are incapable of accurately representing synoptic and sub-synoptic precipitation and mesoscale convective systems. Statistical or dynamic downscaling of GCM outputs using RCMs is generally used to improve the horizontal resolution. When downscaled, however, uncertainties from the host GCM are retained in the statistical model or the embedded RCM (e.g., Hurrell et al. 2009; Wu et al. 2005; Laprise et al. 2012). Additionally, inconsistencies due to the different formulations of physical, chemical, and dynamical processes, and the different resolutions of orography between the downscaled GCM and the RCM can cause inconsistent flow patterns at the lateral boundary points (Leung 2012). Even though the same physical parameterizations are used in both the GCM and the embedded RCM, "resolution-unaware" parameterizations can lead to the simulation of different atmospheric states at different resolutions (e.g., Skamarock et al. 2012; Gustafson et al. 2013). Moreover, nested RCMs are generally incapable of incorporating the two-way interactions between regional and global processes.

High-resolution GCMs are effective in overcoming many of the limitations encountered by coarse resolution GCMs and RCMs. Due to their fine grid-spacing, important processes such as large-scale condensation, land-sea interaction, and topographical forcing are better resolved in high-resolution GCMs (Boyle and Klein 2010). Studies suggest that with increasing horizontal resolution, GCMs are better able to explicitly capture mesoscale convective systems (e.g., Zhao et al. 2009; Manganello et al. 2012), reproduce diurnally forced circulations, represent orographically modulated rainfall (e.g., Boyle and Klein 2010; Lau and Ploshay 2009), and represent extreme precipitation events (Wehner et al. 2014). Since they can resolve mesoscale processes, multi-scale interactions are better represented in high-resolution GCMs (Gent et al. 2010). Unlike RCMs, they also reflect the interplay between regional and global scales. Due to the important role of SST on atmospheric circulation and precipitation patterns the atmospheric GCMs (AGCMs) with prescribed SST and coupled ocean-atmosphere GCMs (CGCMs) with adjusted SST are frequently used to study the dynamic effects of the on-going climate change (He et al. 2014; He and Soden 2015, 2016; Pascale et al. 2017).

The present study makes use of a high-resolution AGCM to analyze the changes in the WAM system and its elements in a warming climate through the end of the 21st century. The evaluation of the model's ability to simulate the past and present climate is the first step towards simulating future. The first part of the study evaluates the ability of High-Resolution Atmospheric Model (HiRAM), a high-resolution AGCM, to simulate WAM at a horizontal resolution of 25 km using a process-based evaluation approach. The evaluation of models is often conducted by comparing the mean state of the model hindcast to observations or reanalyses. However, recent studies highlight the importance of the process-based evaluation to further validate and ensure the ability of the model to represent the key processes and dynamic features that are important in projecting the future changes (James et al. 2015).

The first part of this study examines how well HiRAM simulates the key features embedded within the WAM circulation, their seasonal means and mean annual cycle, and their interactions. In the second part, the future projection of the WAM system, which uses the Representative Concentration Pathway (RCP) 8.5 is analyzed and the changes in the mean state and seasonal evolution of the WAM circulation along with its contributing elements are investigated. A brief review of the model and a detailed description of the experiment setting follows the introduction. The summary and a discussion of the results conclude the paper.

2 Model and experimental setup

HiRAM was developed at the Geophysical Fluid Dynamics Laboratory (GFDL) (Zhao et al. 2009; Gamdt 2004), based on the atmospheric component (AM2) of the GFDL coupled model 2 (CM2). This model uses a cubed-sphere finite-volume dynamical core (Putman and Lin 2007; Lin 2004), and the simulations are conducted at C360 (25 km) horizontal resolution, which is the typical spatial resolution of regional climate downscaling. Compared to AM2, it also has improved vertical resolutions (32 levels) but the same parameterizations, except for deep convection. HiRAM uses a shallow convective scheme for moist convection and stratiform cloudiness (Bretherton et al. 2004) which makes the contribution of the resolved vertical transport more significant, especially in the tropics. Global aerosol forcing is incorporated as monthly climatologies of the five aerosol species (i.e., dust, black carbon, organic carbon, sulfate and sea salt) (Ginoux et al. 2006), which are pre-calculated using

the global chemistry transport model, Model for OZone And Related chemical Tracers (MOZART) (Horowitz et al. 2003). Radiative forcing caused by dust is extremely important for an accurate simulation of the North African summer climate (Bangalath and Stenchikov 2015), yet it is generally not included in many RCMs but is well accounted in our simulations. The model is coupled to the GFDL Land Model 3 (LM3). In the present study, however, we prescribe model equilibrium seasonal vegetation climatology and use prescribed SSTs, both observed and model-generated, as the bottom boundary condition.

Two different Atmospheric Model Intercomparison Project (AMIP)-type simulations have been conducted for the historical period, one forced with observed SSTs from the Hadley Centre Sea Ice and Sea Surface Temperature dataset (HadISST) (Rayner et al. 2003), and the other forced with SST from ESM2M, the Earth System Model (ESM) developed at GFDL, which uses GFDL's Modular Ocean Model (MOM) (Dunne et al. 2012, 2013). These simulations are named HiRAM-obsSST and HiRAM-ESM2M, respectively. Both simulations span a period of 30 years, from 1975 to 2004. The resolution of the parent ESM, which provide the SSTs for HiRAM, is 2.5° longitude by approximately 2° latitude, with 24 vertical levels. Both HiRAM and ESM2M (which provides the SST for HiRAM) are the descendants of the same atmospheric model, AM2. The atmospheric components of ESM2M and HiRAM differ only in the spatial resolution and parameterization of deep convection. ESM2M uses relaxed ArakawaSchubert (RAS) formulation (Moorthi and Suarez 1992) for moist convection. It has been shown, however, that the tropical African precipitation is sensitive to the choice of convective parameterization (Hill et al. 2017), especially over Sahel region. The difference between the climate simulated by ESM2M and HiRAM, therefore, is due to the combined effects of an improved spatial resolution and a modified convective parameterization. The interaction of these two factors is complex and nonlinear as the performance of a convective parameterization is usually scale dependent. This issue is discussed in detail in Hill et al. (2017). To further evaluate the model performance, data from Climate Research Unit (CRU) (Brohan et al. 2006), Global Precipitation Climatology Project (GPCP) (Adler et al. 2003), University of Delaware (Willmott and Matsuura 2001) and ERA-Interim reanalysis (Dee et al. 2011) are used.

To estimate the future changes of WAM, three ensemble simulations, starting from different initial conditions are conducted for the period 2076–2099, using RCP 8.5 emission scenario. The anomalies of the future projections are estimated by using the 1985–2004 reference period from the historical simulations and the statistical significance of the anomalies is estimated using the two-tailed Student's t test. The SST in RCP 8.5 HiRAM simulation is taken from ESM2M RCP8.5 simulations for the same period. Though the simulations cover the entire globe, the present study restricts the analyses to the WAM domain.

3 Results

The WAM is part of the global monsoon system, and the reversal of trade wind direction in the lower troposphere during WAM has been traditionally explained by the thermal contrast between the cooler tropical Atlantic and the heated north African continent. During the boreal Spring (March–June) ITCZ moves across West Africa and the dry, warm, and dusty Harmattan winds are replaced by moisture-laden cold southwesterlies from the tropical Atlantic. These south–westerlies are formed between the Atlantic cold tongue and Saharan Heat Low (SHL) and bring moisture to the continent. The Inter Tropical Discontinuity (ITD) limits the monsoon flow in the north. The monsoon trough, which is collocated with ITD, is flanked by the Azores High and the St. Helena High to the north and the south, respectively. WAM is a complex system comprised of several multiscale processes ranging from planetary to cumulus scales (Hall and Peyrille 2006) and influenced by coastlines (Nicholson 2009) and circulations driven by orography (Sultan and Janicot 2003). This makes the horizontal model resolution an important constraint on the accurate simulation of WAM.

The most prominent elements of the WAM system include the African Easterly Jet (AEJ) and the associated African Easterly Waves (AEWs), the Tropical Easterly Jet (TEJ), the Saharan Heat Low (SHL) and the Inter-Tropical Convergence Zone (ITCZ). The intensity and position of these features control the amount of rainfall and its variability revealing strong scale interactions between the different elements of WAM (Redelsperger et al. 2002). Therefore, the ability of a climate model to simulate WAM greatly depends on its representation of the interaction between these multi-scale processes. Although many models simulate the overall pattern of WAM adequately well, they often fail to simulate many of the important features such as the onset of WAM, the intensity of rainfall, especially over the Sahel, and the rainfall maxima associated with orography. For example, there is no consistency between models on both the magnitude and even sign of the future rainfall changes over West Africa (Cook and Vizy 2006; Roehrig et al. 2013). In the following section, we evaluate how the time mean structure and temporal evolution of various structural elements of WAM are simulated in HiRAM and analyze the benefit of using a finer resolution model.

3.1 Precipitation

3.1.1 Summer climatology

WAM begins in April with intense rainfall over the Gulf of Guinea, and the rainfall shifts to the Sahel by the end of June (Hagos and Cook 2007). The mean JJAS (June, July, August, and September) rainfall is concentrated between 5°N and 12°N. The most striking result to emerge from the WAM rainfall climatology (Fig. 1) is that HiRAM simulates the position and the width of the rainbelt more accurately than coarse resolution parent ESM2M. ESM2M (Fig. 1e) overestimates the rainfall with a wider rainband which extends northward up to 18°N causing enhanced precipitation over the Sahel, whereas in both HiRAM simulations, HiRAM-ESM2M and HiRAM-obsSST (Fig. 1d, f), the rainbelt is mostly confined between 5°N and 15°N, and is closer to observations. Patches of high precipitation are observed over elevated regions such as Guinea Highlands, Jos Plateau and Cameroon Mountains in both GPCP and CRU datasets. These orographic rainfall maxima are well-resolved in HiRAM simulations but are absent in ESM2M simulation due to its coarse spatial resolution.

However, in the HiRAM simulations an anomalous increase in precipitation of ~ 2 mm/day is seen in the equatorial Atlantic over the marine ITCZ region; also, the 850 hPa wind increases over the same region which may be attributed to the enhanced convection over marine ITCZ. Many studies have identified this as an inherent problem of AGCMs (e.g., Richter and Xie 2008). HiRAM-ESM2M simulation also exhibits wet bias over the Gulf of Guinea. A similar wet bias over the same region was found by Siongco et al. (2015) in the high-resolution AGCMs. This increased precipitation is often associated with the anomalous westerlies resulting from misrepresentation of the Atlantic cold tongue and most GCMs suffer from it (Richter and Xie 2008; Zermeno-Diaz and Zhang 2013). This could be a plausible reason for the wet bias in HiRAM-ESM2M run. The Atlantic cold tongue over the Gulf of Guinea drives the WAM rainfall towards the African continent. Colder SSTs along the coast cause the reduction in sensible and latent heat fluxes, which in turn stabilizes the atmosphere and hence suppress convection. The Atlantic cold tongue also intensifies the cross-equatorial southerlies, pushing the rainband inland (Okumura and Xie 2004). HiRAM-ESM2M SST (Fig. 2c) is ~ 2 K warmer than that in HiRAM-obsSST simulation (Fig. 2b).

3.1.2 Annual cycle

WAM has three distinct phases: the onset period (March–May), the high rain period (June–August) and the southward retreat (September–October) (Le Barbe et al. 2002). During the onset period, the rainbelt expands north from the coast to 4°N. By the end of June, the rainbelt abruptly shifts north again from 4°N to 10°N, marking the beginning of the high rain season in the Sahel, and ending of heavy rain over the Guinean coast. This northward migration of the rainbelt is called the monsoon jump (Sultan and Janicot 2003). The southward retreat, which is the last phase of the WAM annual cycle, begins in September. Figure 3 shows the annual cycle of precipitation from observations, reanalysis, and model simulations. In ESM2M simulation (Fig. 3e) rainbelt extends farther northward by ~ 2 degrees and the monsoon jump is delayed with the rainbelt shifting north in late July and shows a wet bias during the high rain period (JJA) when compared to observations. Generally for HiRAM runs the width of the rain belt shrinks compared to the ESM2M run giving a more accurate annual cycle pattern. HiRAM-obsSST (Fig. 3d) produces the annual precipitation pattern that is most consistent with the GPCP and ERA-Interim precipitation, though a wet bias is present throughout the season. HiRAM-ESM2M (Fig. 3f) also displays wet biases during June and July. A remarkable difference between HiRAM-obsSST and other simulations is that HiRAM-obsSST simulation is able to produce the drying of Guinean Coast during the high rain period, which emphasizes the importance of the SST pattern on WAM rainfall.

3.2 Saharan heat low (SHL)

The Saharan heat low (SHL), an important element of WAM, is a zonally elongated trough rather than a circular low and is thought to be an extension of the planetary-scale Asian monsoon trough (Wu et al. 2009). In the lower troposphere, the southwesterly monsoon flow is intensified by the cyclonic circulation associated with the SHL, along its eastern flank, while the northeasterly Harmattan flow is supplemented along its western flank (Parker et al. 2005). Orographic features such as the Atlas and Hoggar mountains play an important role in the seasonal evolution of SHL (Lavaysse et al. 2009). Hence, an accurate representation of the processes associated with these orographic features is essential for the precise simulation of SHL. Figure 4 shows the seasonal mean surface air temperature climatology from the observations, reanalysis, and GCM runs; the overlaid contours represent the mean sea level pressure. We find that HiRAM reproduces detailed fine-scale orographic features, such as temperature minima over the Jos Plateau and the Hoggar and Tibesti Mountains (Fig. 4d, f), better than the coarse-resolution ESM2M run (Fig. 4e). When compared with the CRU (Fig. 4a) and the University of Delaware (Fig. 4b) data, the ERA-Interim reanalysis (Fig. 4c) overestimates the temperature over SHL by ~ 1.5 K. The SHL temperature represented in HiRAM simulations is closer to the observations while ESM2M underestimates the SHL temperature by ~ 2 K compared with observations and HiRAM simulations.

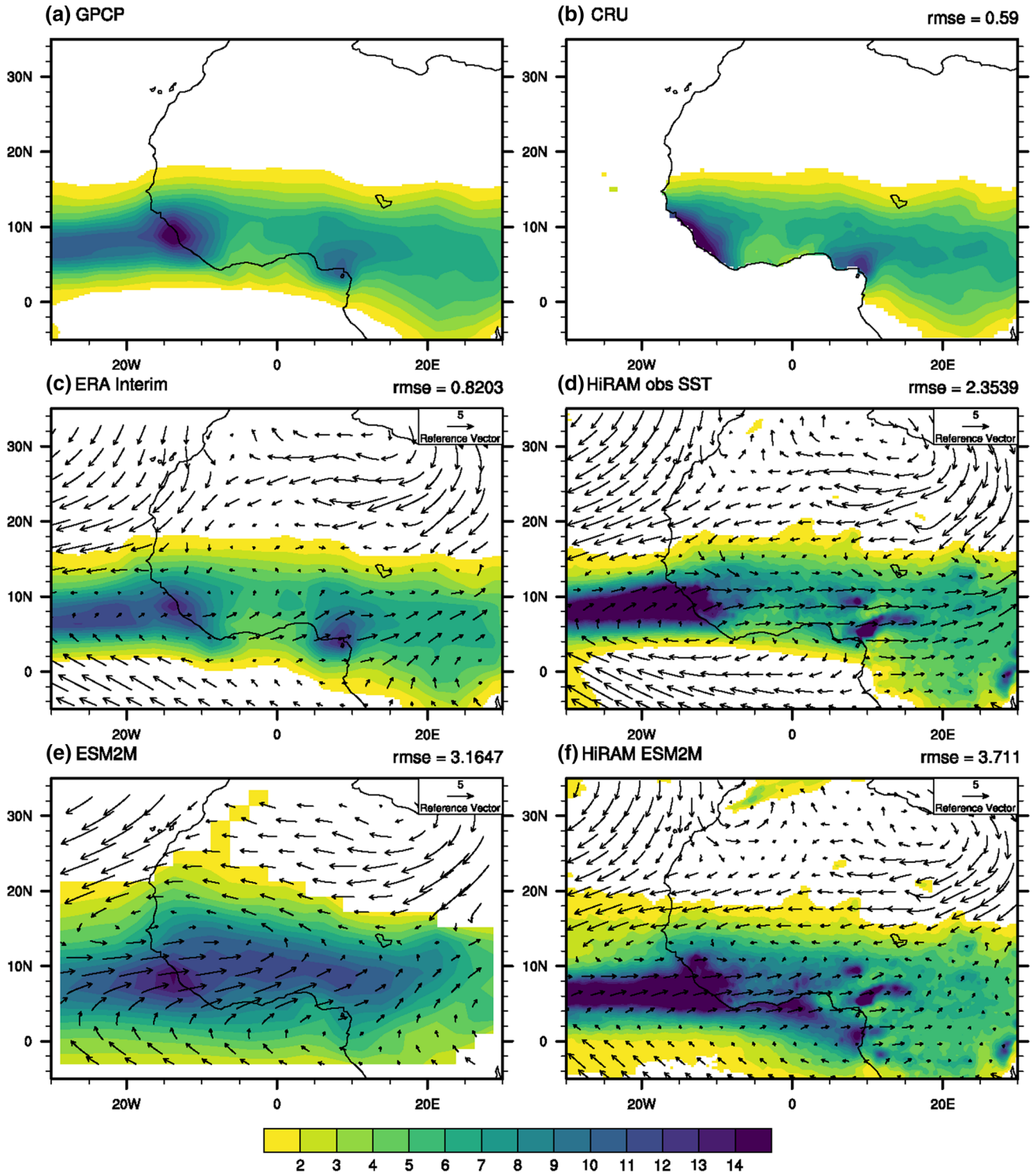

Fig. 1 Seasonal mean precipitation rate (filled contours; mm/day) and 850 hPa wind (vectors, m/s) from **a** GPCP; **b** CRU; **c** ERA Interim; **d** HiRAM-obsSST; **e** ESM2M; **f** HiRAM-ESM2M averaged over June–September (JJAS) for the period 1974–2004. Wind reference vector is 5 m/s. Precipitation RMSE is calculated with respect to GPCP

In the ESM2M simulation, SHL appears as a narrower and more northward positioned belt of high temperature. In the ERA-Interim reanalysis, two closed-off pressure contours are observed over the northwestern and eastern Sahara. According to McCrary et al. (2014b, 2014a), though the seasonal SHL mean appears to be a circular contour in the

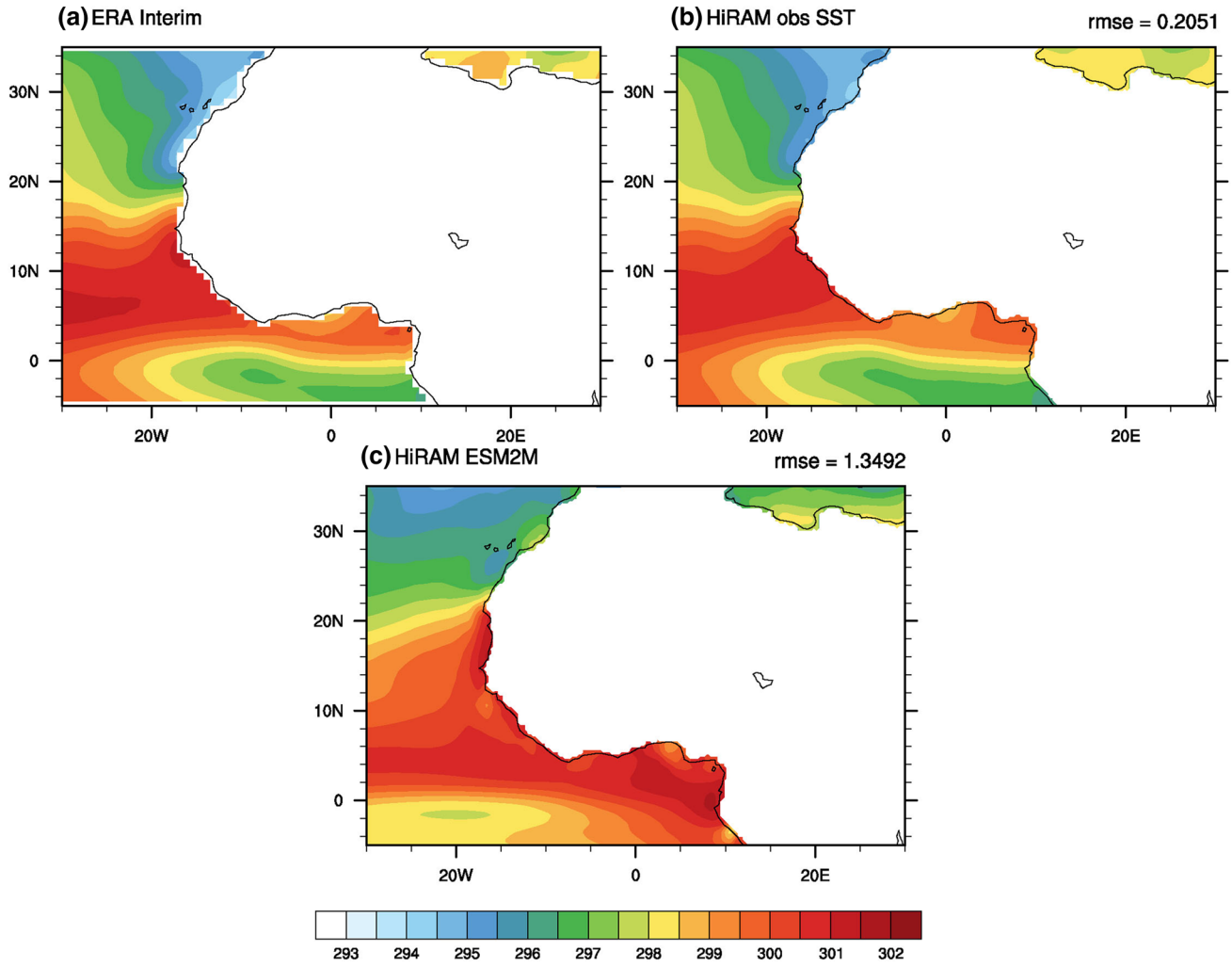

Fig. 2 Seasonal average SSTs (K) for JJAS from **a** ERA Interim; **b** HiRAM-obsSST; **c** HiRAM-ESM2M for the period 1974–2004

ERA Interim reanalysis, an elongated SHL is observed on a day-to-day basis. HiRAM-ESM2M simulation depicts a similar circular low over the eastern Sahara, while an elongated heat low appears in HiRAM-obsSST run.

The seasonal evolution of SHL is depicted in Fig. 5. Both observations (Fig. 5a, b) and reanalysis (Fig. 5c) exhibit the migration of SHL from the Sahel in March-April to the Sahara in June–August. HiRAM simulations (Fig. 5d, f) reproduce the migration of SHL though with a reduced intensity. In the ESM2M simulation (Fig. 5e) intensity of SHL over the Sahel is especially low, which partly explains the reduction in MAM rainfall in the ESM2M simulation (Fig. 3e). The southward retreat of SHL, during SON, is absent in ESM2M simulation.

SHL plays a pivotal role in developing and maintaining AEJ, another key feature of WAM system. Lower tropospheric warming due to SHL results in shallow meridional circulation. The equatorward branch of this circulation accelerates AEJ through the conservation of the angular momentum at 700 hPa (Thorncroft and Blackburn 1999). Fig. 6 shows the vertical cross section of the omega ($\omega = \frac{dp}{dt}$) and omega-meridional wind vectors. Omega is scaled to match the magnitude of the meridional wind and its sign is reversed so that the positive values represent vertical motion. In ERA-Interim reanalysis (Fig. 6a), two distinct cells of vertical motion are visible: the deeper cell, confined between 4°N and 10°N associates with the moist convection over monsoon rainbelt, and the shallower cell, which is centered around 20°N, links to the dry convection over SHL. HiRAM successfully simulates these two convection cells, contrary to ESM2M. The positions of these two cells in HiRAM simulations (Fig. 6b, d) are similar to those in the ERA-Interim reanalysis. HiRAM overestimates the monsoon convection and underestimates the vertical motion associated with dry convection over SHL. The two cells are almost indistinguishable

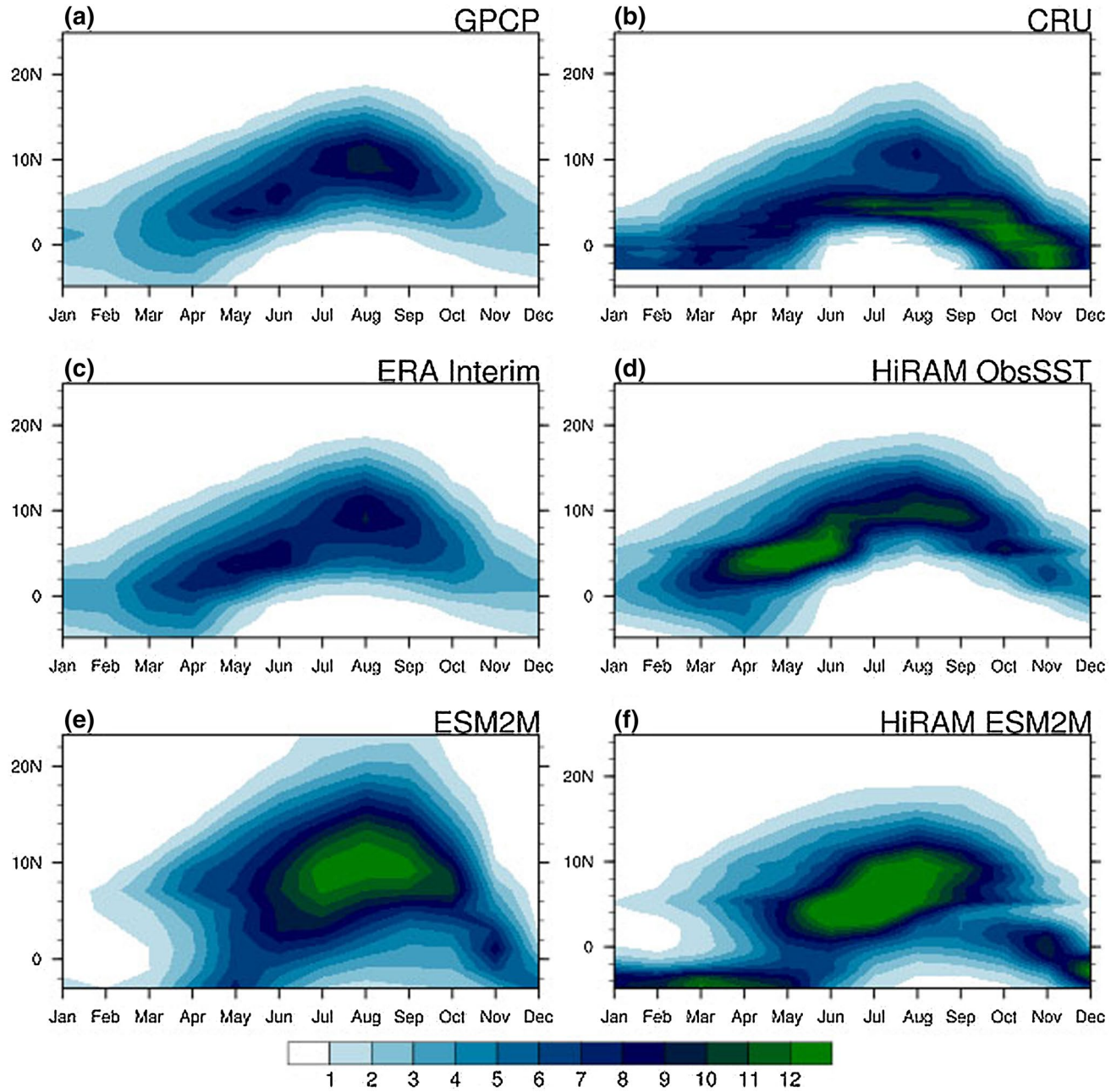

Fig. 3 Latitude- time cross-section of precipitation rate (mm/day) averaged between 15W and 10E from **a** GPCP; **b** CRU; **c** ERA Interim; **d** HiRAM-obsSST; **e** ESM2M; **f** HiRAM-ESM2M for the period 1974–2004

in ESM2M simulation (Fig. 6c), and their positions are shifted northward, potentially impacting the representation of AEJ. The northerly return flow of the shallow meridional circulation contributes to the intensity and position of AEJ. In the ERA-Interim reanalysis, this northerly flow is centered around 15°N and extends from 800 to 500 hPa. In HiRAM-ESM2M the northerly return flow of the shallow meridional circulation is weaker and shallower, and that in HiRAM-obsSST simulation is closer to the ERA-Interim reanalysis. This northerly flow is entirely absent in ESM2M run. A more detailed discussion of the AEJ is provided in Sect. 3.3. The shallow meridional circulation associated with SHL is also a decisive control of the Sahel rainfall. Strengthening of the shallow meridional circulation and the associated dry outflow from SHL inhibits the northward progress of the Sahel rainfall (Peyrille et al. 2007; Zhang et al. 2008; Shekhar and Boos 2017; Zhai and Boos 2017).

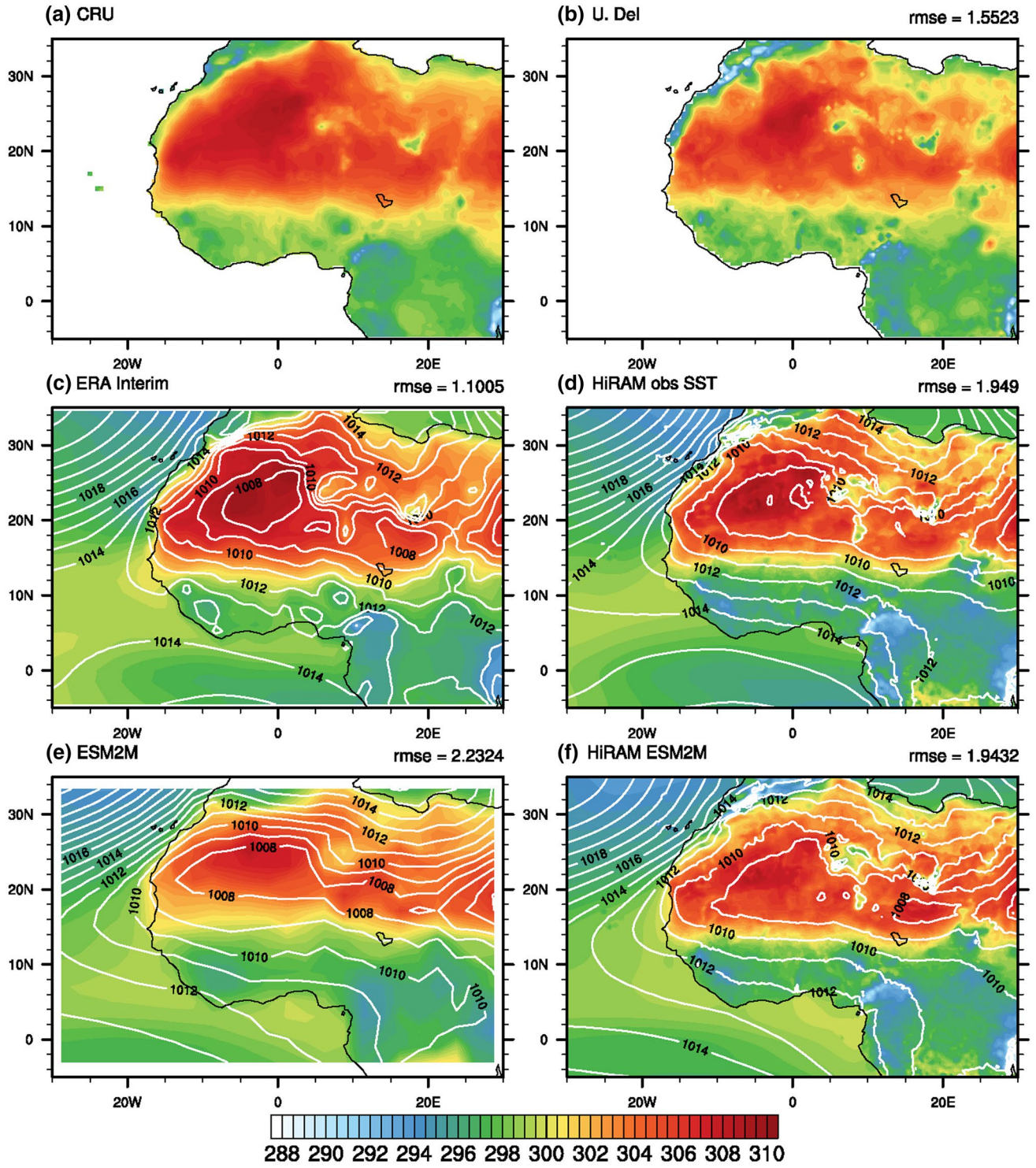

Fig. 4 Seasonal (JJAS) mean of surface air temperature (filled contours; K) and mean sea level pressure (line contours; hPa) from **a** CRU; **b** U. Del **c** ERA Interim; **d** HiRAM-obsSST; **e** ESM2M; **f** HiRAM-ESM2M for the period 1974–2004. Temperature RMSE is calculated with respect to CRU.

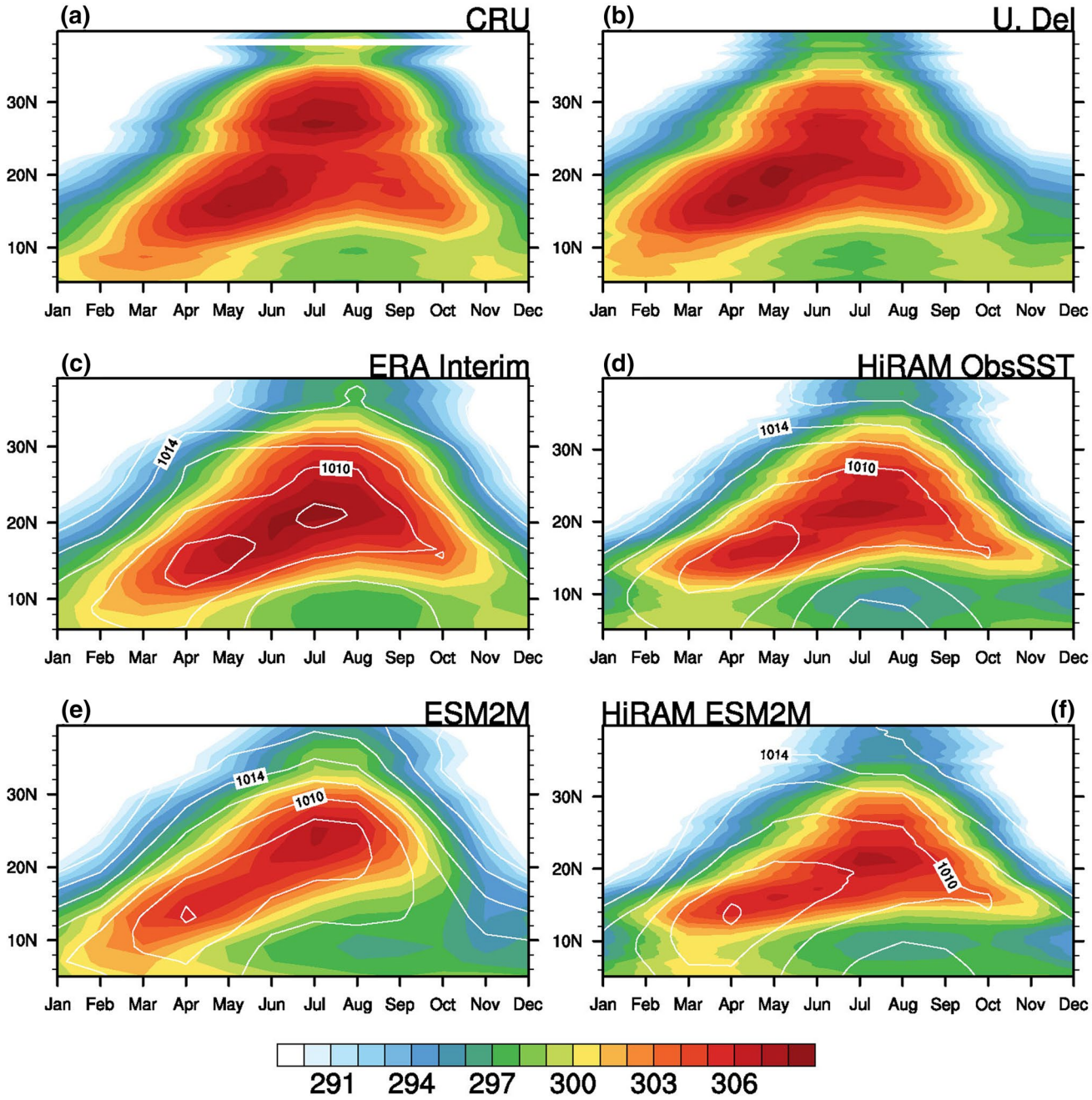

Fig. 5 Latitude–time cross-section of surface air temperature (filled contours; K) and mean sea level pressure (line contours; hPa) averaged between 15W and 10E from **a** CRU; **b** U. Del **c** ERA Interim; **d** HiRAM obSST; **e** ESM2M; **f** HiRAM-ESM2M averaged over JJAS for the period 1974–2004

3.3 African easterly jet (AEJ)

The AEJ is formed due to the strong thermal contrast between the Sahara and the Atlantic Ocean and is maintained by the juxtaposition of a moist convection to the south and a dry convection to the north (Nicholson 2013). It has a mid-tropospheric (600–700 hPa) core with strong zonal winds (up to $\sim$ 10 m/s) and spans from east to West Africa. The WAM rainbelt is also the loci of Mesoscale Convective Systems (MCS) associated with the African Easterly Waves (AEWs), which form along the flanks of AEJ. The cloud clusters asscociated with AEWs are the main rain producing systems of WAM (Nicholson and Grist 2003). AEWs are, mostly, found in a latitudinal belt near and south of the AEJ and this zone corresponds to the region between the axes of the AEJ and the

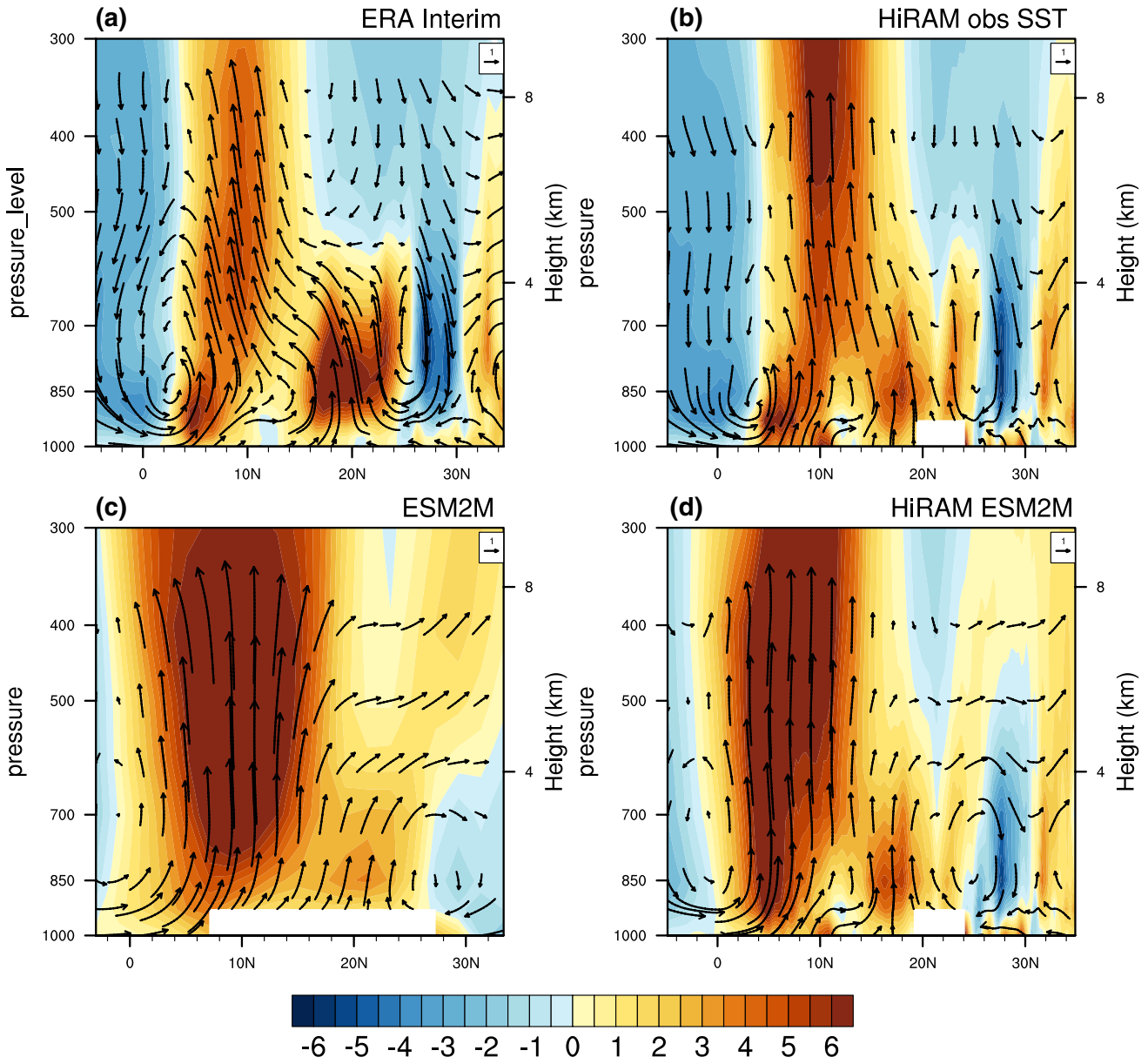

Fig. 6 Latitude–height cross-section of omega (filled contours; Pa/s) and omega-v vector (vectors; Pa/s-scaled) averaged between 15W and 10E from **a** ERA Interim; **b** HiRAM-obsSST; **c** ESM2M; **d** HiRAM-ESM2M averaged over JJAS for the period 1974–2004. Omega is scaled to match the value of meridional wind and its sign is reversed so that positive values represent ascending motion

upper-tropospheric TEJ, though some AEWs form on the northern flank of AEJ (Tourre 1981).

The influence of the AEJ on the WAM rainfall is complex. The strengthening of the AEJ is generally associated with a decrease in WAM precipitation. But, according to Newell and Kidson (1984), the stronger AEJ is an effect, rather than a cause, of reduced rainfall. The latitudinal position of the AEJ is more important than its strength in deciding the amount of WAM rainfall. During the wet years, the jet is displaced northward and baroclinic instability is strong over the Sahel, in contrast, it is weaker in this region during the dry years (Nicholson and Webster 2007). A more equatorward position of the AEJ often corresponds to a decrease in rainfall over the Sahel (Jenkins et al. 2005; Nicholson 2008). The zonal wind speed at 600 hPa is shown in Fig. 7, solid lines indicate AEJ axes. ESM2M simulation overestimates the jet speed over land by $\sim$ 2 m/s. Although HiRAM-ESM2M shows a narrow positive wind speed bias over the Sahel, it positions jet axes closer to the ERA-Interim reanalysis. When comparing the HiRAM simulations, HiRAM-obsSST has the closest to the ERA-Interim the zonal wind pattern at 600 hPa. The ESM2M run exhibits a northward shift of AEJ

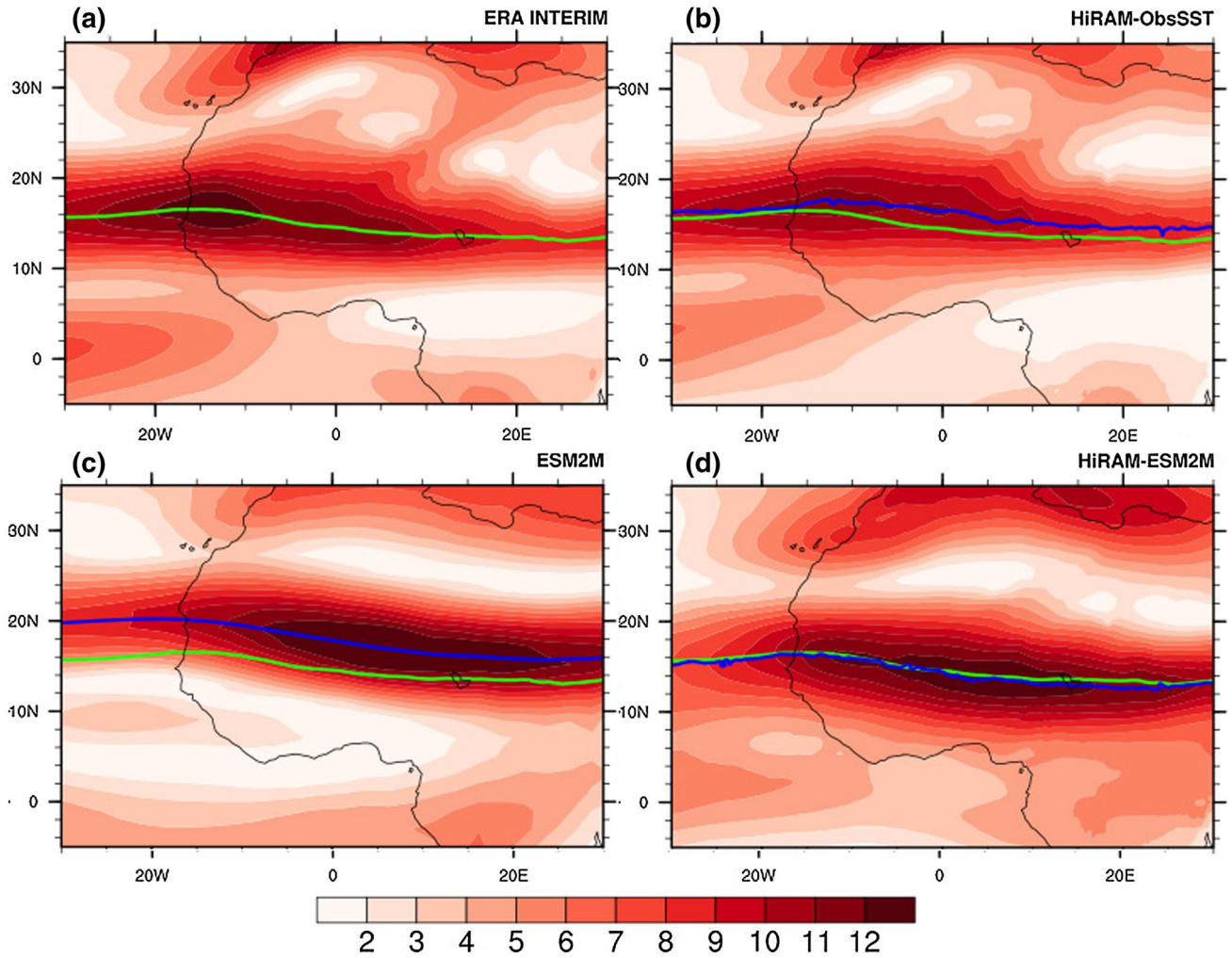

Fig. 7 Zonal wind speed at 600 hPa (filled contours; m/s) from **a** ERA Interim; **b** HiRAM-obsSST; **c** ESM2M; **d** HiRAM-ESM2M averaged over JJAS for the period 1974–2004. Solid lines represent jet axes; green is jet axis from ERA Interim and blue is jet axis from the respective simulation

axes by ~ 2°; this shift combined with an overestimation of AEJ intensity might be the cause of the wet bias found in ESM2M simulation. On the other hand, HiRAM simulations correctly position the AEJ axis, which results in a narrower, and more accurate rain belt (see Fig. 1d, f, h).

The surface meridional temperature gradient is a key factor in the latitudinal position of the AEJ (Wu et al. 2009), with positive gradients corresponding to the AEJ (Fig. 8). The ESM2M run (Fig. 8c) underestimates the surface meridional temperature gradient; the positive gradients extend further north when compared with those in the observations (Fig. 8a, b) or in the ERA-Interim reanalysis (Fig. 8c). The HiRAM simulations, owing to the higher horizontal resolution, (Fig. 8d, f) simulate a more detailed structure of the temperature gradient and the pattern, especially the positive gradient band which corresponds to AEJ, is more similar to the observations. The better rainfall pattern in HiRAM simulations can be attributed to the fine structure of the surface meridional temperature gradient which, in turn, corrects the latitudinal position of AEJ.

The vertical cross-section of zonal winds in the ERA-Interim reanalysis depicts AEJ as closed contours centered at 600 hPa and around 15°N (Fig. 9a). HiRAM simulations (Fig. 9b, d) reproduce intensity and vertical and latitudinal positions of the AEJ reasonably well, whereas the ESM2M simulation (Fig. 9c) exhibits a weaker AEJ, shifted northward. Similarly to the WAM rainbelt and the SHL, but in a more subtle way, the AEJ too undergoes a seasonal migration from south to north. In the ERA-Interim reanalysis (Fig. 10a) AEJ reaches its peak intensity starting in May through September. This pattern is reproduced by HiRAM-obsSST run, with slightly reduced winds (Fig. 10b). However, the ESM2M simulation exhibits northward shift of AEJ during the peak intensity period (Fig. 10c). Duration

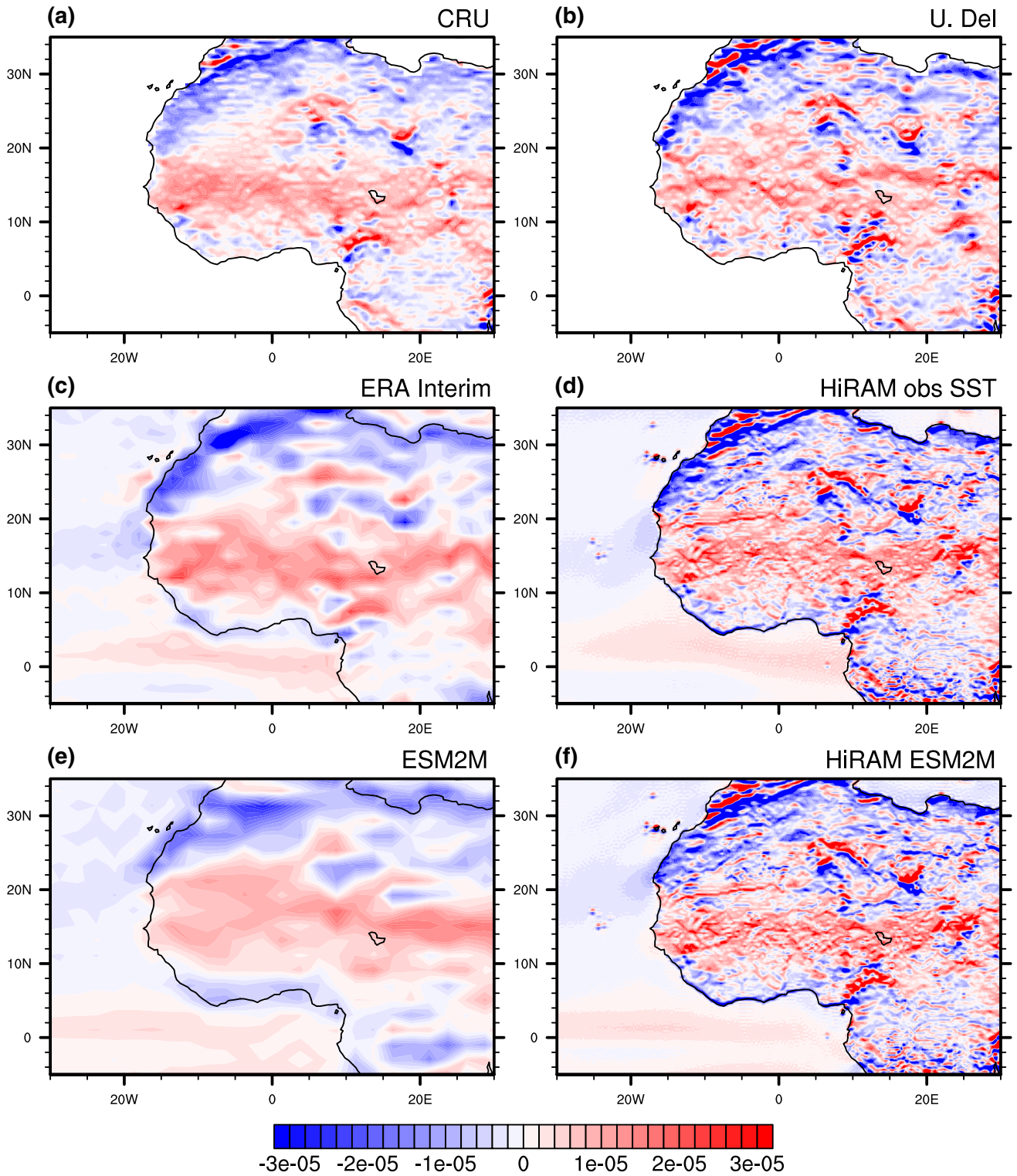

Fig. 8 Meridional gradient of surface air temperature (filled contours; K/m) from **a** CRU; **b** U. Del **c** ERA Interim; **d** HiRAM-obsSST; **e** ESM2M; **f** HiRAM-ESM2M averaged over JJAS for the period 1974–2004

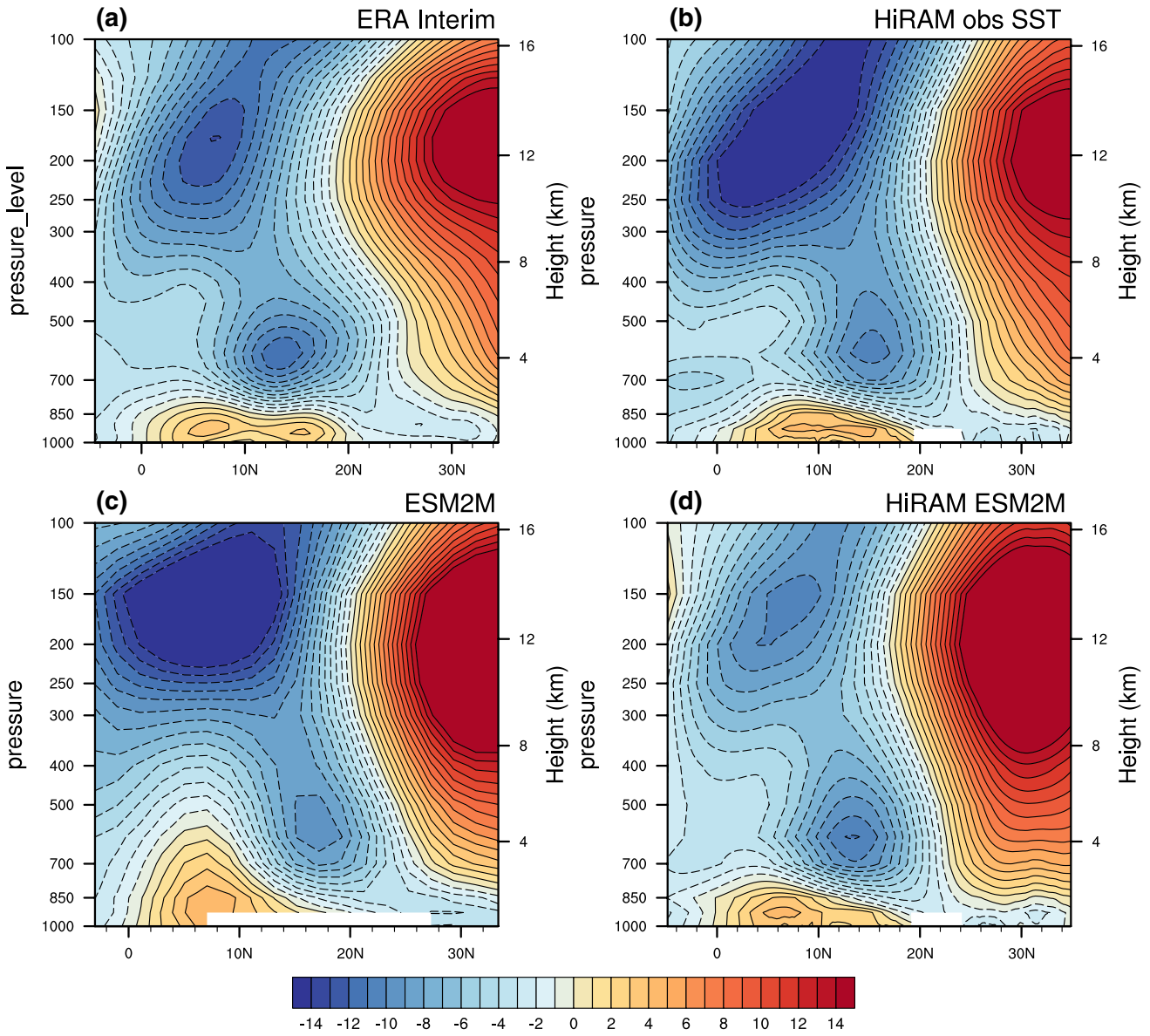

Fig. 9 Latitude–height cross-section of zonal wind (filled contours; m/s) averaged between 15W and 10E from **a** ERA; Interim **b** HiRAM-obsSST; **c** ESM2M; **d** HiRAM-ESM2M averaged over JJAS for the period 1974–2004

of maximum winds in HiRAM-ESM2M simulation is shorter than HiRAM-obsSST simulation or the ERA Interim reanalysis.

3.4 Monsoon flow and the West African westerly jet (WAWJ)

The tropical Atlantic is the main moisture source for the WAM and the moisture is transported inland by low-level westerlies. This westerly flow, known as the West African Westerly Jet (WAWJ), is located near 10°N along the West African coast and has a maximum speed of 6 m/s. It was first identified by Grodsky et al. (2003), using satellite observations. There are two distinctive low level westerly flow regimes, which are the primary moisture carriers of the WAM: the westerly component of monsoon flow and the WAWJ (Fig. 9a). The WAWJ forms at the beginning of June and dissipates around mid-October, reaching its maximum strength in August (Pu and Cook 2010). The westerlies are an important control in determining the latitude of the AEJ, and therefore of the tropical rainbelt. Strong westerlies displace the AEJ northward over the Sahel (Nicholson and Webster 2007). The ESM2M run shows strong westerlies reaching up to 600 hPa (Fig. 9c), which push AEJ northward, while ERA-Interim (Fig. 9a) and HiRAM

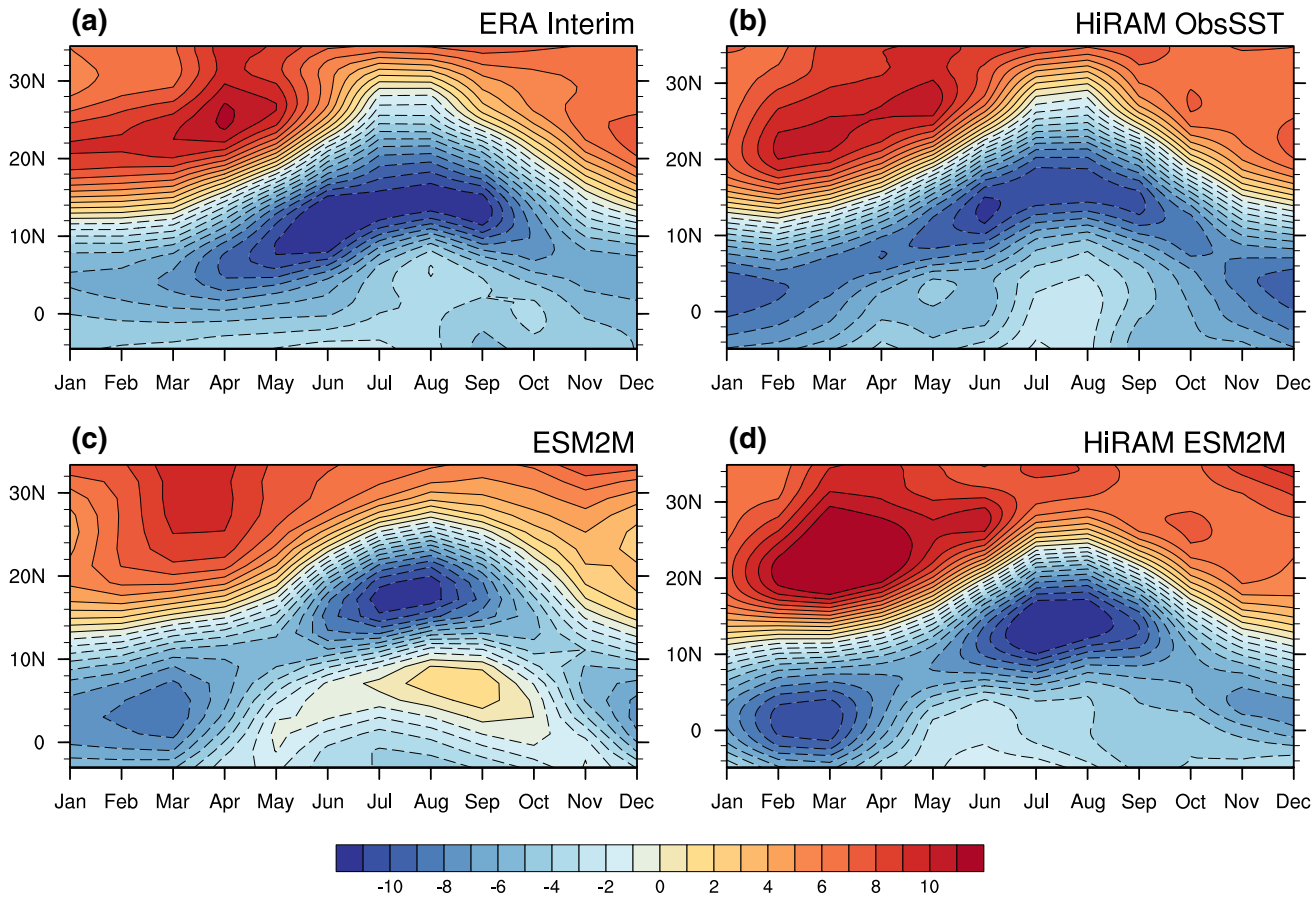

Fig. 10 Latitude–time cross-section of zonal wind (filled contours; m/s) at 700 hPa averaged between 15W and 10E from **a** ERA Interim; **b** HiRAM-obsSST; **c** ESM2M; **d** HiRAM-ESM2M averaged over JJAS for the period 1974–2004

simulations (Fig. 9b, d) show a shallower band of westerlies extending up to 850 hPa. The seasonal climatology of 925 hPa wind is shown in Fig. 11. WAWJ is seen as the westerly flow over Guinean Coast (near 10°N) in ERA-Interim data (Fig. 11a). Both HiRAM-ESM2M and HiRAM-obsSST overestimate the strength of WAWJ (Fig. 11b, d), while ESM2M not only overestimates its strength but extends its position to the west (Fig. 11c).

3.5 WAM onset

It is challenging for the GCMs and RCMs to accurately predict WAM onset. Different indicators have been used to define the WAM onset in the past (e.g., Sijikumar et al. 2006; Fontaine and Louvet 2006; Vellinga et al. 2013; Diaconescu et al. 2015). The present study uses a local onset index similar to that introduced by Diaconescu et al. (2015). This index is based on the occurrence of wet days, and duration and intensity of rainy periods. Onset index in a particular year is calculated as the next day of the minimum of daily rainfall accumulated anomalies. The daily accumulated rainfall anomalies (A) at each grid point are estimated as,

$$A(day) = \sum_{n=1^{st}January}^{day} (R(n) - \mathbf{R}) \quad (1)$$

where $R(n)$ represents the daily rainfall. **R** is the climatological mean of rainfall at each grid point if it is above 1 mm/day. If it is less than 1 mm/day, **R** is fixed to 1 mm/day. This method of onset estimation is effective in avoiding the isolated rain events followed by dry spells and in providing a more meaningful measure compared to conventional definitions of onset. The Monsoon onset index is calculated for the period 1997–2004, over 12°N–20°N and 15°W–15°E.

Figure 12 shows the monsoon onset index in GPCP, ESM2M simulation, and HiRAM simulations. In the GPCP dataset, the WAM onset occurs during 100–120 Julian days in the southern Sahel, and during 150–160 Julian days in Central Sahel (Fig. 12a). ESM2M simulation produces an early onset in both southern and Central Sahel (90–110 Julian days and 120–140 Julian days respectively) when

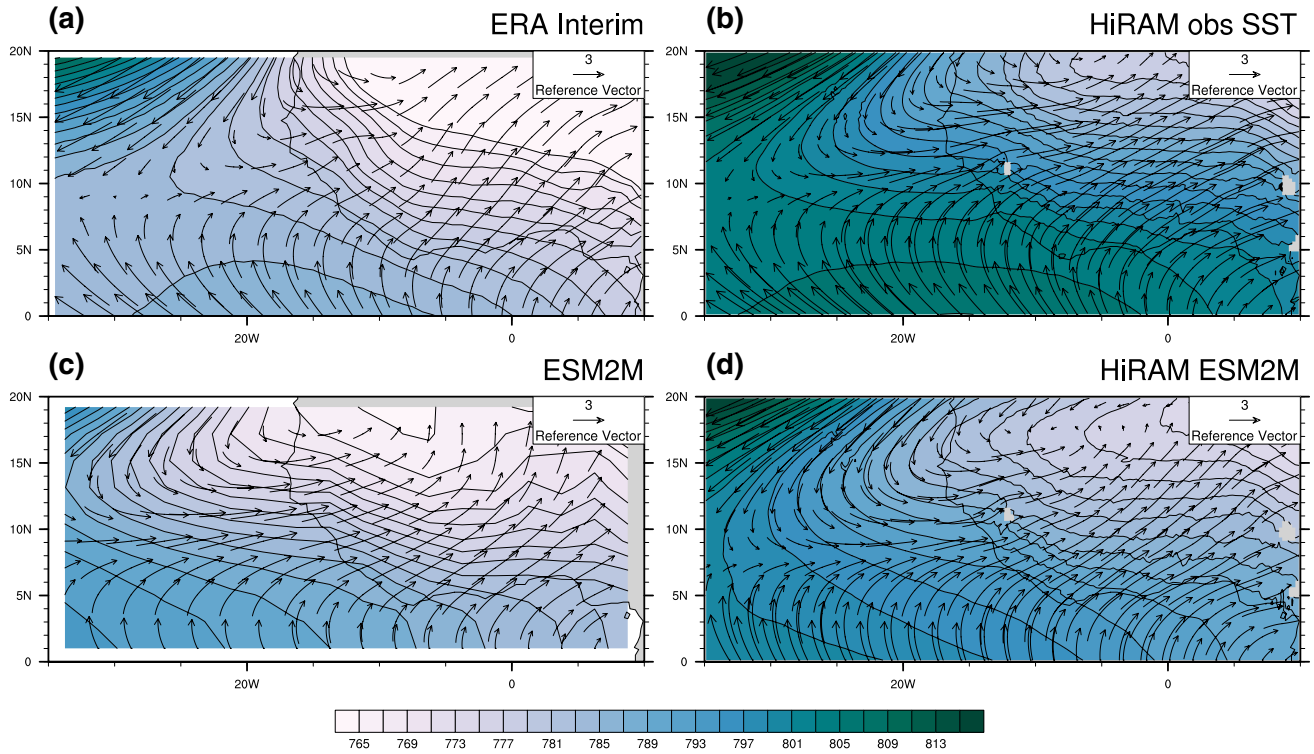

Fig. 11 Geopotential height at 925 hPa (filled contours; m) and 925 hPa wind (vectors; m/s) from **a** ERA Interim; **b** HiRAM-obsSST; **c** ESM2M; **d** HiRAM-ESM2M averaged over JJAS for the period 1974–2004. Wind reference vector is 3 m/s

compared to observation (Fig. 12c). In general, HiRAM simulations better reproduce the overall pattern of progression of WAM onset from south to north when compared with their parent ESM. While HiRAM-obsSST simulation exhibits an early onset in the southern Sahel (Fig. 12b), HiRAM-ESM2M displays a similar pattern to that of GPCP dataset (Fig. 12d). Both HiRAM simulations show an early onset in the eastern Sahel.

3.6 Climate change projections

As mentioned above, there is a wide range of disagreement among models on the behavior of WAM rainfall in the 21st-century projections. Inter-model disagreements on WAM rainfall projections which are present in both CMIP3 and CMIP5 simulations can possibly be due to the inability of the coarse resolution GCMs to resolve convective rainfall (e.g., Biasutti et al. 2008; Druyan 2011; Fontaine et al. 2011; Roehrig et al. 2013). In this regard, it is particularly relevant to examine the effect of high the spatial resolution of HiRAM on WAM projections.

The changes of 2m temperature, precipitation rate, and seasonal cycle of precipitation between the end and the beginning of the 21st century are shown in Fig. 13. The entire domain experiences warming during JJAS (Fig. 13a) and the temperature change in elevated regions, such as the Atlas, Hoggar, and Tibesti mountains exceeds 4 K with a maximum warming over the Atlas Mountains. The Sahel and the southwestern Sahara also experience warming; a distinctive belt of warming centered around is 18°N.It should also be noted that the equatorial Atlantic experience warming of > 3 K. However, the land warming is stronger and the increase of the land-ocean temperature gradient causes the restructuring of WAM dynamics (Bathiany et al. 2014).

The precipitation anomalies are characterized by increased precipitation over the equatorial Atlantic Ocean and the Guinean coast, but they produce contrasting anomalies over the Sahel (Fig. 13b). Increased precipitation over the equatorial Atlantic and Guinean coast can be attributed to the warmer SST in these regions (Fig. 3S). However, the Gulf of Guinea experiences reduction of precipitation. Southern Sahel experiences drying with a distinct band of reduced precipitation centered around 10°N. It is also noteworthy that some parts of the western Sahara experience an increase in precipitation.

The anomalies of the annual cycle of precipitation rate from the reference period are shown in the Fig. 13c. Intense drying is observed during the pre-monsoon months. During the monsoon months, precipitation increases over a band centered around 5°N, with decreased rainfall on either side. It is evident that the Sahel experiences drying throughout the monsoon season, although a slight increase in precipitation

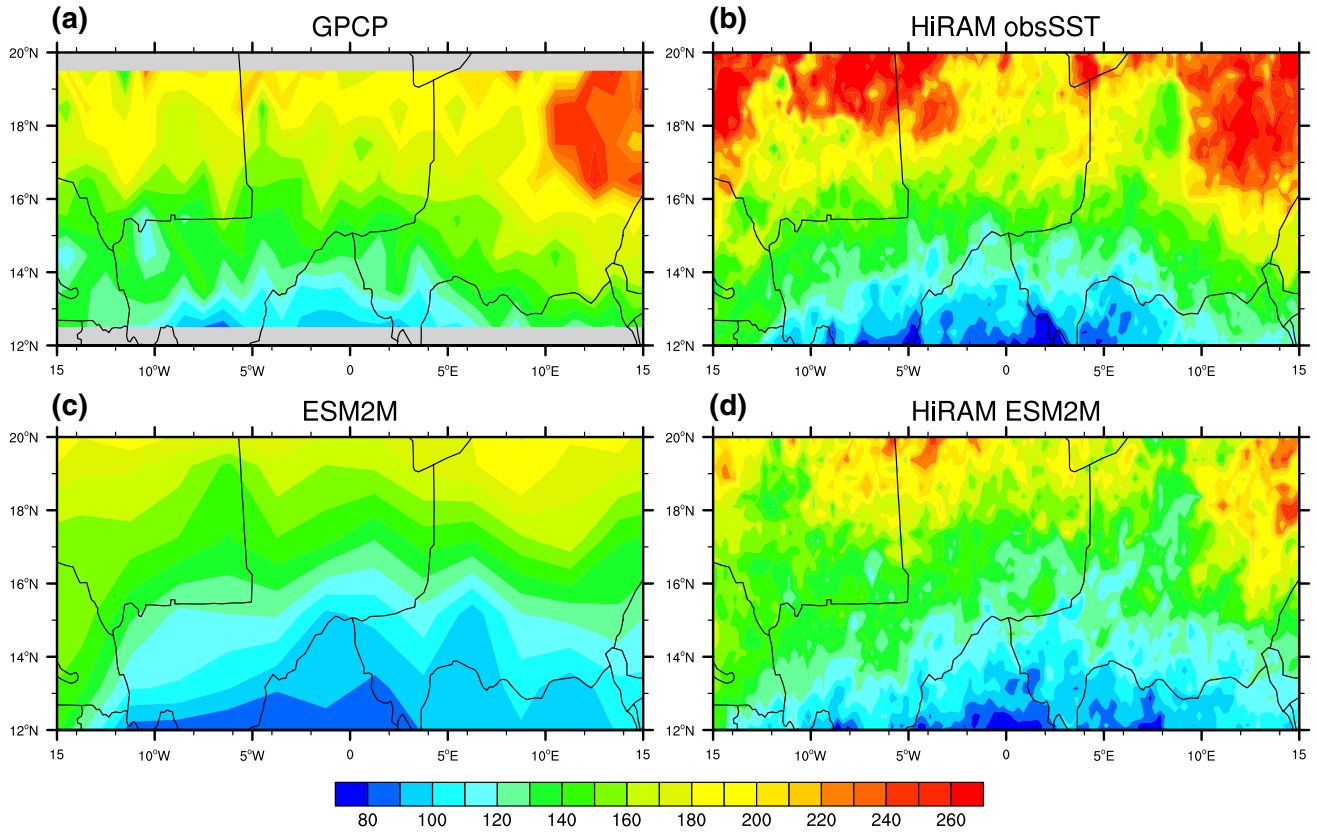

Fig. 12 Average local onset index (Julian day) over Sahel for the period 1997–2004, in Julian day, **a** GPCP; **b** HiRAM-obsSST; **c** ESM2M; **d** HiRAM-ESM2M

can be seen during late May and early June. It should be also noted that the whole domain experiences a significant increase in precipitation during the early winter.

In the RCP 8.5 projection, by the end of the 21st century the moist convection cell over the WAM rainbelt shrinks but exhibits a more intensified core of upward motion (Fig. 14). A band of decreased updraft centered around 12°N is found which results in the drying of Sahel. The dry convection cell which belongs to SHL exhibits a slight increase in intensity due to the warming of Sahara. As mentioned before, strengthening of the shallow meridional circulation associated with SHL could lead to decreased Sahel rainfall. This could be the plausible reason for the drier Sahel seen in Fig. 13b. The position of AEJ does not exhibit any significant change (Fig. 15). The southern flank of the AEJ shows a significant increase in the intensity and this intensification is stronger over the eastern parts of the domain.

The response of the WAM onset date by the end of 21st century is shown in Fig. 16. The monsoon onset is delayed up to 2 weeks or more over most parts of the domain except a few negative response patches over West African coastal zones. Biasutti and Sobel (2009) observed a similar pattern in CMIP3 models and attributed it to the delayed annual cycle of tropical Atlantic SST. The response has an east–west gradient with stronger response (more than 2 weeks) over central and eastern Sahel compared to western Sahel. In other words, the central and eastern Sahel will experience a later monsoon onset than the western Sahel in the future.

4 Summary and conclusions

Horizontal resolution is a significant constraint on the accuracy of simulating synoptic- and sub-synoptic-scale rainfall using GCMs. In the present study, we use the high-resolution AGCM HiRAM with a horizontal grid spacing of 25 km, forced by present and future SST from earth system model ESM2M, to simulate WAM under the present and future climate conditions. To assess the efficacy of HiRAM in simulating WAM, a process-based assessment method is employed. In general, HiRAM improves the simulation of the WAM compared with the parent model, ESM2M. However, HiRAM simulations overestimate precipitation over the marine ITCZ. Positive rainfall rate anomalies appear over the Gulf of Guinea in HiRAM-ESM2M which is corrected in

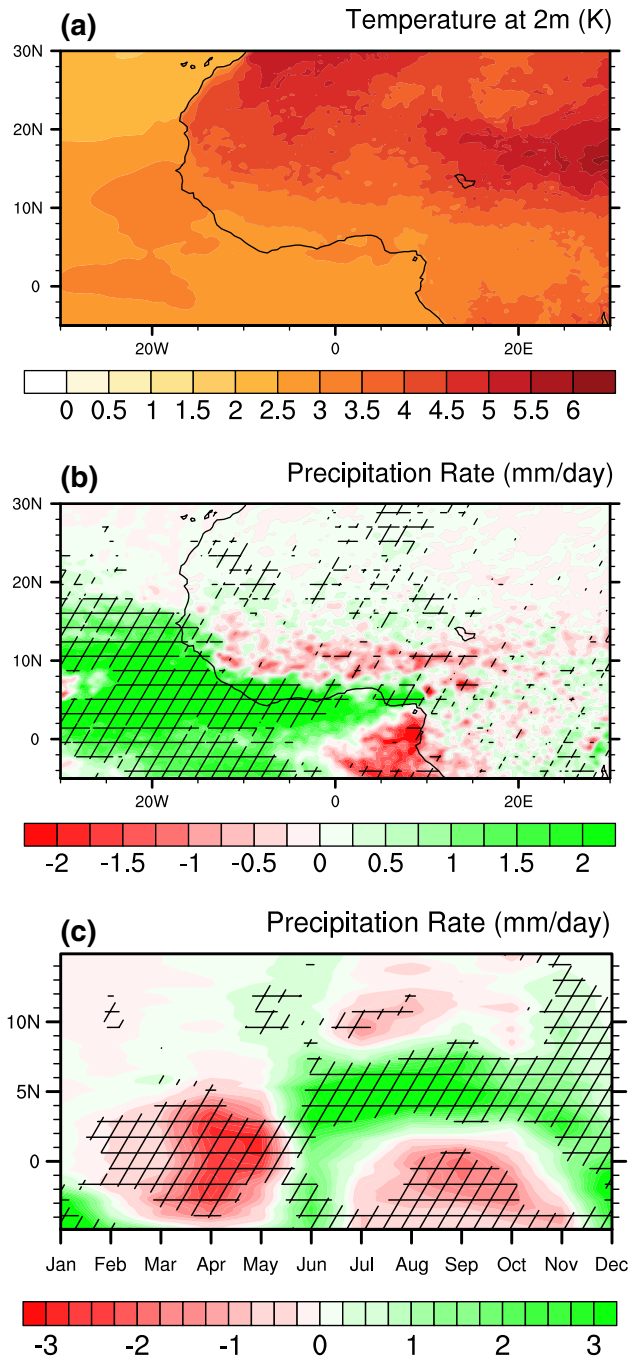

Fig. 13 Projected changes in HiRAM RCP 8.5 by the end of 21st century in, **a** mean summer (JJAS) 2-m temperature (K), only values with at least 95% significance level are plotted; **b** mean summer (JJAS) precipitation rate (mm/day), hatching shows the areas where the anomalies are statistically significant at least at 95% level; **c** latitude–time cross-section of annual precipitation rate (mm/ day) cycle averaged between 15W and 10E, hatching shows the areas where the anomalies are statistically significant at least at 90% level. Anomalies are calculated by subtracting mean of variables in the historical period (1985–2004) from that of future (2080–2099)

HiRAM-obsSST run. High rainfall rates in HiRAM-ESM2M over the Gulf of Guinea might originate from the misrepresentation of the Atlantic cold tongue in the ESM2M simulation. Due to its fine resolution, HiRAM is able to simulate orographic rainfall maxima in all three simulations. The pattern of the annual rainfall cycle is well simulated in HiRAM runs and HiRAM-obsSST produces the annual cycle pattern which is closest to observations, with the distinct drying of Guinean coast during high rain period, though a wet bias is observed during June–July.

The SHL is better represented in HiRAM simulations than in the ESM2M run. In the ESM2M simulation, the placement of the SHL is shifted northward, which may explain the northward expansion of the rainband in this run. Two separate convection cells, moist and dry, representing the monsoon rainbelt and SHL respectively, are well-represented in HiRAM simulations, whereas the ESM2M simulates only a single cell. The shallow meridional flow associated with the SHL is not captured in the ESM2M simulation, but it is well-resolved in HiRAM simulations; HiRAM-obsSST run is closest to observations. This feature is very important for the accurate simulation of intensity and position of AEJ, which is an important control of intensity and northward extent of the rainbelt. One of the most salient results of our study is the representation of the AEJ axis in HiRAM simulations. When compared with the ESM2M simulations, the position of the jet axis is much closer to observations in HiRAM simulations; this can be attributed to the better representation of the meridional temperature gradient due to the higher horizontal resolution. The equatorward position of the AEJ axis, when compared with the ESM2M run, is responsible for the accurate two-cell convection structure of WAM in HiRAM simulations. In the ESM2M run, the northward position of the AEJ axis pushes the moist convection cell north, causing the moist and dry convection cells to merge. The northward position of AEJ in the ESM2M simulations could be caused by the poor representation of the WAWJ. Analysis of the WAM onset shows that the onset time in HiRAM simulations is closer to the gridded observations than the parent ESM2M, which simulates the WAM onset $\sim$ 20 days earlier than observed.

The process-based analysis reveals that HiRAM improves the representation of WAM elements compared to the parent ESM owing to its high spatial resolution and the modified convective parameterization, which attests to its ability to predict future climate. In the RCP 8.5 scenario, elevated areas of Sahel and western Sahara experience a robust warming of > 4 K by the end of the 21st century. Precipitation increases over the equatorial Atlantic and the Guinean coast, while the southern Sahel appears drier. At the same time, western Sahara experiences a moderate increase of precipitation. The monsoon onset exhibits early WAM onset

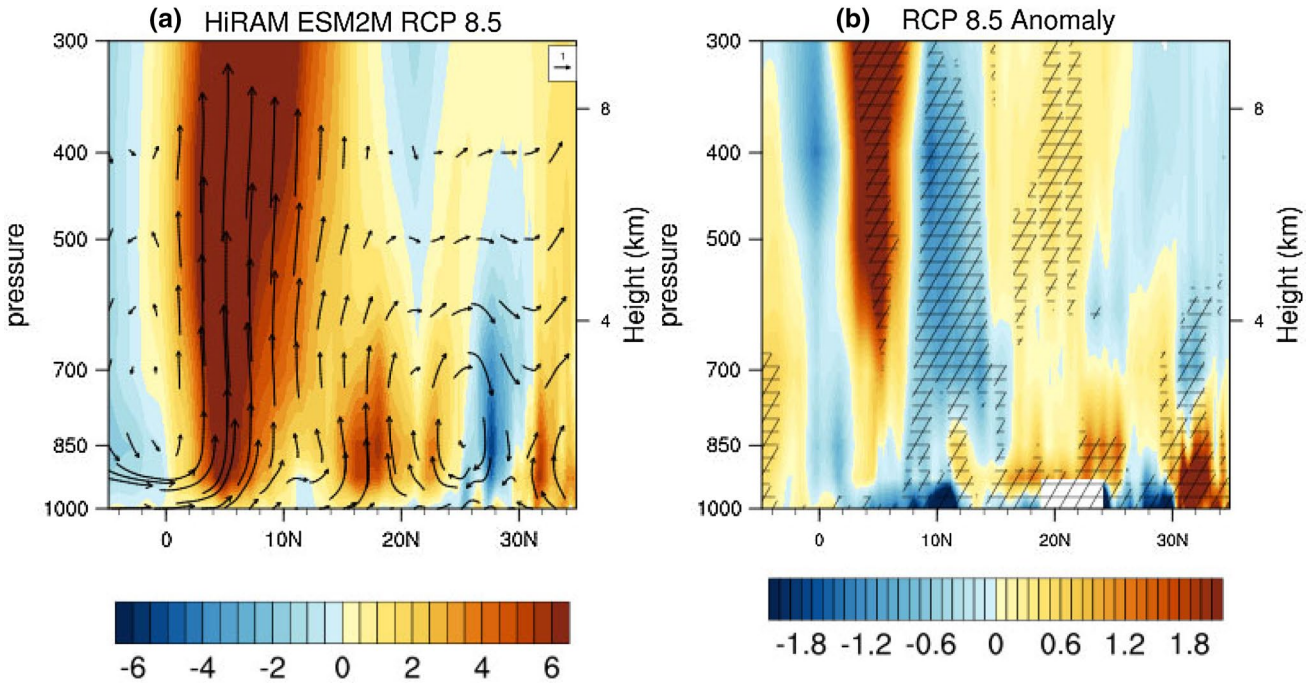

Fig. 14 Latitude–height cross-section of omega (filled contours; Pa/s) and omega-v vector (vectors; Pa/s-scaled) averaged between 15W and 10E from **a** HiRAM RCP 8.5 JJAS climatology; **b** HiRAM RCP 8.5 mean anomaly of 2080–2099 period from 1985 to 2004 period, hatching shows the areas where the anomalies are statistically significant at least at 90% level. Omega is scaled to match the value of meridional wind and its sign is reversed so that positive values represent ascending motion

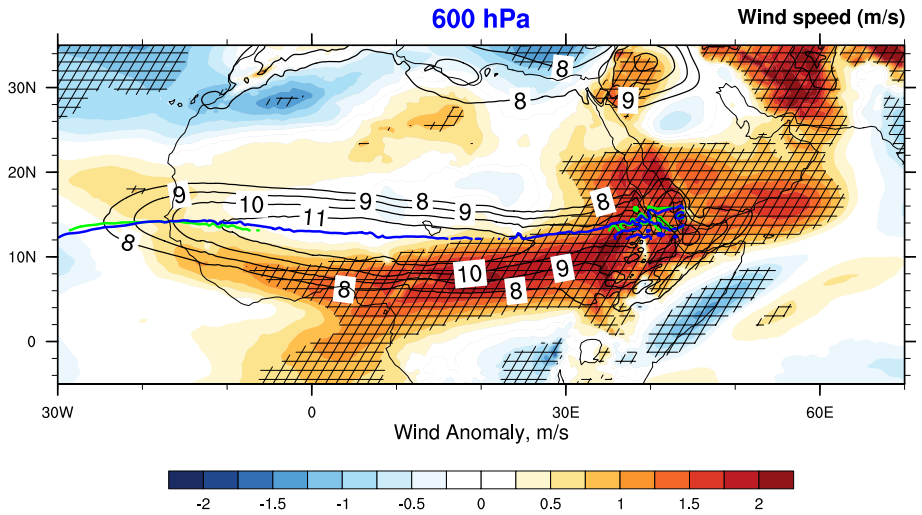

Fig. 15 Mean zonal wind speed anomaly at 600 hPa of (2080–2099)–(1985–2004) (filled contours; m/s) from HiRAM RCP 8.5 projection, averaged over JJAS.Hatching shows the areas where the anomalies are statistically significant at least at 90% level. Solid lines represent jet axes; green is jet axis from reference period and blue is jet axis from respective projection. The black contours represent seasonal mean of zonal wind

over the eastern parts of the domain and delayed onset over western parts.

The high horizontal resolution of the model is instrumental in simulating many WAM features such as jet axes, circulations driven by orography, and precipitation forced by coastal uplift. The fine resolution of HiRAM, along with the modified convective parameterization, are the main reasons for its better simulation of WAM than the parent ESM2M. Also, the differences among HiRAM simulations demonstrate the important role of SST in these features. This study, however, does not account for the climate-vegetation feedback as it uses a climatological vegetation cover which does not respond to CO_2 and temperature/precipitation changes. It should also be noted that recently there are also attempts to use thermodynamic tracers such as moist static energy or equivalent potential temperature for diagnosing the monsoon circulation, instead of temperature (Bordoni and Schneider 2008; Hurley and Boos 2013). However, such

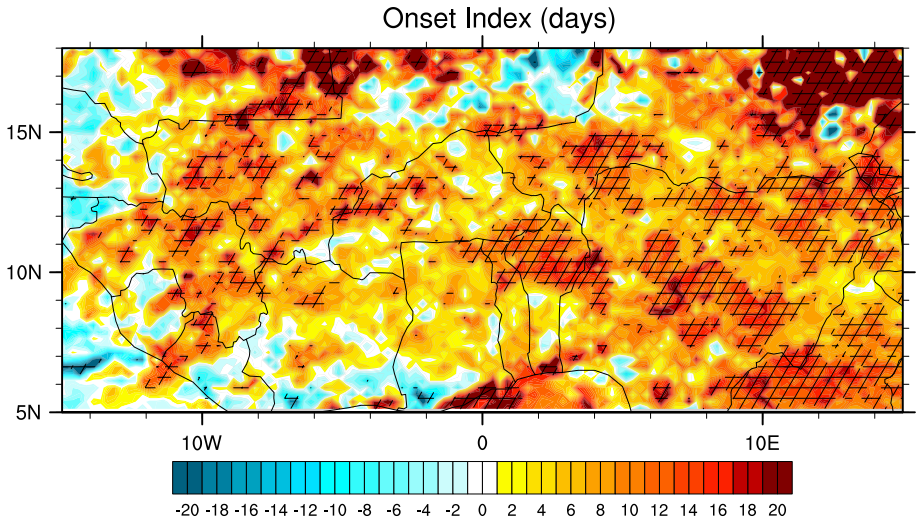

Fig. 16 Average local onset index anomaly over Sahel for (2080–2099)–(1985–2004), in Julian day, from HiRAM RCP 8.5. Hatching shows the areas where the anomalies are statistically significant at least at 90% level

an analysis is not addressed in the present paper. Synoptic scale features such as AEWs are also beyond the scope of this study but are planned as an extension of this work.

Acknowledgements We thank V. Ramaswamy, M. Zhao, B. Wyman, and C. Kerr of GFDL for their assistance with acquiring and using HiRAM model. The research reported in this publication was supported by funding from King Abdullah University of Science and Technology (KAUST). For computer time, this research used the resources of the KAUST Supercomputing Laboratory, Thuwal, Saudi Arabia. The simulations and figures are available from the authors upon request. The GPCP Precipitation data provided by the NOAA/OAR/ESRL PSD, Boulder, Colorado, USA, are available at: http://www.esrl.noaa.gov/psd/ and the HadCRUT data are available at: http://www.metoffice.gov.uk/hadobs/hadcrut3/.

References

Adler RF, Huffman GJ, Chang A, Ferraro R, Xie PP, Janowiak J, Rudolf B, Schneider U, Curtis S, Bolvin D (2003) The version-2 global precipitation climatology project (gpcp) monthly precipitation analysis (1979–present). J Hydrometeorol 4(6):1147–1167. https://doi.org/10.1175/1525-7541(2003)004

Bangalath HK, Stenchikov G (2015) Role of dust direct radiative effect on the tropical rainbelt over middle east and north Africa: a high resolution agcm study. J Geophys Res Atmos 120:4564–4584. https://doi.org/10.1002/2015JD023122

Barros V, Field C, Dokke D, Mastrandrea M, Mach K, Bilir T, Chatterjee M, Ebi K, Estrada Y, Genova R, et al (2015) Climate change 2014: impacts, adaptation, and vulnerability. Part B: regional aspects. Contribution of working group II to the fifth assessment report of the intergovernmental panel on climate change. Cambridge University Press, pp 1199–1265

Bathiany S, Claussen M, Brovkin V (2014) Co2-induced sahel greening in three cmip5 earth system models. J Clim 27(18):7163–7184. https://doi.org/10.1175/jcli-d-13-00528.1

Biasutti M, Held IM, Sobel AH, Giannini A (2008) Sst forcings and sahel rainfall variability in simulations of the twentieth and twenty-first centuries. J Clim 21(14):3471–3486. https://doi.org/10.1175/2007JCLI1896.1

Biasutti M, Sobel AH (2009) Delayed sahel rainfall and global seasonal cycle in a warmer climate. Geophys Res Lett. https://doi.org/10.1029/2009GL041303

Boko MI, Niang A, Nyong C, Vogel A, Githeko M, Medany B, Osman-Elasha R, Tabo, P, Yanda (2007) Climate change 2007: impacts, adaptation and vulnerability. Contribution of working group II to the fourth assessment report of the Intergovernmental Panel on Climate Change, Cambridge University Press, Cambridge UK, pp 433–467 **(chap Africa)**

Boone A, Decharme B, Guichard F, de Rosnay P, Balsamo G, Beljaars A, Chopin F, Orgeval T, Polcher J, Delire C (2009) The amma land surface model intercomparison project (ALMIP). Bull Am Meteorol Soc 90(12):1865–1880

Bordoni S, Schneider T (2008) Monsoons as eddy-mediated regime transitions of the tropical overturning circulation. Nat Geosci 1(8):515–519. https://doi.org/10.1038/ngeo248

Boyle J, Klein SA (2010) Impact of horizontal resolution on climate model forecasts of tropical precipitation and diabatic heating for the twp-ice period. J Geophys Res Atmos (1984–2012) 115:4. https://doi.org/10.1029/2010JD014262/full

Bretherton CS, McCaa JR, Grenier H (2004) A new parameterization for shallow cumulus convection and its application to marine subtropical cloud-topped boundary layers. Part I: Description and 1d results. Mon Weather Rev 132(4):864–882

Brohan P, Kennedy JJ, Harris I, Tett SF, Jones PD (2006) Uncertainty estimates in regional and global observed temperature changes: a new data set from 1850. J Geophys Res Atmos 111:D12. https://doi.org/10.1029/2005JD006548

Cook KH, Vizy EK (2006) Coupled model simulations of the west African monsoon system: twentieth-and twenty-first-century simulations. J Clim 19(15):3681–3703

Cornforth R (2012) Overview of the west African monsoon 2011[1]. Weather 67(3):59–65

Dee D, Uppala S, Simmons A, Berrisford P, Poli P, Kobayashi S, Andrae U, Balmaseda M, Balsamo G, Bauer P (2011) The era-interim reanalysis: configuration and performance of the data assimilation system. Q J R Meteorol Soc 137(656):553–597

Diaconescu EP, Gachon P, Scinocca J, Laprise R (2015) Evaluation of daily precipitation statistics and monsoon onset/retreat over western Sahel in multiple data sets. Clim Dyn 45(5–6):1325–1354

Druyan LM (2011) Studies of 21st-century precipitation trends over west Africa. Int J Climatol 31(10):1415–1424. https://doi.org/10.1002/joc.2180

Druyan LM, Feng J, Cook KH, Xue Y, Fulakeza M, Hagos SM, Konare A, Moufouma-Okia W, Rowell DP, Vizy EK (2010) The wamme regional model intercomparison study. Clim Dyn 35(1):175–192

Dunne JP, John JG, Adcroft AJ, Griffies SM, Hallberg RW, Shevliakova E, Stouffer RJ, Cooke W, Dunne KA, Harrison MJ (2012) GFDLS ESM2 global coupled climate-carbon earth system models. Part I: Physical formulation and baseline simulation characteristics. J Clim 25(19):6646–6665

Dunne JP, John JG, Shevliakova E, Stouffer RJ, Krasting JP, Malyshev SI, Milly P, Sentman LT, Adcroft AJ, Cooke W (2013) GFDLS ESM2 global coupled climate-carbon earth system models. Part II: Carbon system formulation and baseline simulation characteristics. J Clim 26(7):2247–2267

Fontaine B, Louvet S (2006) Sudan-sahel rainfall onset: definition of an objective index, types of years, and experimental hindcasts. J Geophys Res Atmos 111:D20

Fontaine B, Roucou P, Monerie PA (2011) Changes in the African monsoon region at medium-term time horizon using 12 AR4 coupled models under the A1B emissions scenario. Atmos Sci Lett 12(1):83–88. https://doi.org/10.1002/asl.321

Gamdt G (2004) The new gfdl global atmosphere and land model AM2-LM2: evaluation with prescribed SST simulations. J Clim 17:4641–4673. https://doi.org/10.1175/JCLI-3223.1

Gent PR, Yeager SG, Neale RB, Levis S, Bailey DA (2010) Improvements in a half degree atmosphere/land version of the CCSM. J Clim 34(6):819–833

Ginoux P, Horowitz LW, Ramaswamy V, Geogdzhayev IV, Holben BN, Stenchikov G, Tie X (2006) Evaluation of aerosol distribution and optical depth in the geophysical fluid dynamics laboratory coupled model CM2. 1 for present climate. J Geophys Res Atmos (1984–2012) 111:D22. https://doi.org/10.1029/2005JD006707

Giorgi F, Jones C, Asrar GR (2009) Addressing climate information needs at the regional level: the cordex framework. World Meteorol Org Bull 58(3):175

Grodsky SA, Carton JA, Nigam S (2003) Near surface westerly wind jet in the Atlantic ITCZ. Geophys Res Lett 30(19). http://onlinelibrary.wiley.com/doi/10.1029/2003GL017867/pdf; http://onlinelibrary.wiley.com/doi/10.1029/2003GL017867/full

Gustafson WI, Ma PL, Xiao H, Singh B, Rasch PJ, Fast JD (2013) The separate physics and dynamics experiment (spade) framework for determining resolution awareness: a case study of microphysics. J Geophy Res Atmos 118(16):9258–9276

Hagos SM, Cook KH (2007) Dynamics of the west African monsoon jump. J Clim 20(21):5264–5284. https://doi.org/10.1175/2007JCLI1533.1

Hall NM, Peyrille P (2006) Dynamics of the west African monsoon. J Phys IV (Proc) EDP Sci 139:81–99

He J, Soden BJ (2015) Anthropogenic weakening of the tropical circulation: the relative roles of direct Co2 forcing and sea surface temperature change. J Clim 28(22):8728–8742. https://doi.org/10.1175/jcli-d-15-0205.1

He J, Soden BJ (2016) The impact of SST biases on projections of anthropogenic climate change: a greater role for atmosphere-only models? Geophys Res Lett 43(14):7745–7750. https://doi.org/10.1002/2016gl069803

He J, Soden BJ, Kirtman B (2014) The robustness of the atmospheric circulation and precipitation response to future anthropogenic surface warming. Geophys Res Lett 41(7):2614–2622. https://doi.org/10.1002/2014gl059435

Hill SA, Ming Y, Held IM, Zhao M (2017) A moist static energy budget-based analysis of the sahel rainfall response to uniform oceanic warming. J Clim 30(15):5637–5660. https://doi.org/10.1175/jcli-d-16-0785.1

Horowitz LW, Walters S, Mauzerall DL, Emmons LK, Rasch PJ, GranierC Tie X, Lamarque JF, Schultz MG, Tyndall GS (2003) A globalsimulation of tropospheric ozone and related tracers: description and evaluation of mozart, version 2. J Geophys Res Atmos (1984–2012) 108:D24. https://doi.org/10.1029/2002JD002853

Hourdin F, Musat I, Grandpeix JY, Polcher J, Guichard F, Favot F, Marquet P, Boone A, Lafore JP, Redelsperger JL (2010) Amma-model intercomparison project. Bull Am Meteorol Soc 91(1):95–104

Hurley JV, Boos WR (2013) Interannual variability of monsoon precipitation and local subcloud equivalent potential temperature. J Clim 26(23):9507–9527. https://doi.org/10.1175/jcli-d-12-00229.1

Hurrell J, Meehl GA, Bader D, Delworth TL, Kirtman B, Wielicki B (2009) A unified modeling approach to climate system prediction. Bull Am Meteorol Soc 90(12):1819–1832

James R, Washington R, Jones R (2015) Process-based assessment of an ensemble of climate projections for west Africa. J Geophys Res Atmos 120(4):1221–1238

Jenkins GS, Gaye AT, Sylla B (2005) Late 20th century attribution of drying trends in the sahel from the regional climate model (REGCM3). Geophys Res Lett 32:22

Jones C, Giorgi F, Asrar G (2011) The coordinated regional downscaling experiment: cordex-an international downscaling link to CMIP5. Clivar Exchang 16(2):34–40

Laprise R, Kornic D, Rapaic M, Separovic L, Leduc M, Nikiema O, Di Luca A, Diaconescu E, Alexandru A, Lucas-Picher P et al (2012) Considerations of domain size and large-scale driving for nested regional climate models: impact on internal variability and ability at developing small-scale details. Springer, Berlin

Lau NC, Ploshay JJ (2009) Simulation of synoptic-and subsynoptic-scale phenomena associated with the east Asian summer monsoon using a high-resolution GCM. Mon Weather Rev 137(1):137–160. https://doi.org/10.1175/2008MWR2511.1

Lavaysse C, Flamant C, Janicot S, Parker D, Lafore JP, Sultan B, Pelon J (2009) Seasonal evolution of the west African heat low: a climatological perspective. Clim Dyn 33(2–3):313–330

Le Barbe L, Lebel T, Tapsoba D (2002) Rainfall variability in west Africa during the years 1950–1990. J Clim 15(2):187–202

Leung LR (2012) Encyclopedia of sustainability science and technology, vol Regional Climate Models. Springer, New York, pp 7365–7381

Lin SJ (2004) A "vertically lagrangian" finite-volume dynamical core for global models. Mon Weather Rev 132(10):2293–2307. https://doi.org/10.1175/1520-0493(2004)132

Manganello JV, Hodges KI, Kinter JL III, Cash BA, Marx L, Jung T, Achuthavarier D, Adams JM, Altshuler EL, Huang B (2012) Tropical cyclone climatology in a 10-km global atmospheric GCM: toward weather-resolving climate modeling. J Clim 25(11):3867–3893

McCrary RR, Randall DA, Stan C (2014a) Simulations of the west African monsoon with a superparameterized climate model. Part I: The seasonal cycle. J Clim 27(22):8303–8322

McCrary RR, Randall DA, Stan C (2014b) Simulations of the west African monsoon with a superparameterized climate model. Part II: African easterly waves. J Clim 27(22):8323–8341

Moorthi S, Suarez MJ (1992) Relaxed arakawa-schubert: a parameterization of moist convection for general circulation models. Mon Wea Rev 120:978–1002. https://doi.org/10.1175/1520-0493(1992)120<0978:RASAPO>2.0.CO;2

Newell RE, Kidson JW (1984) African mean wind changes between sahelian wet and dry periods. J Climatol 4(1):27–33. https://doi.org/10.1002/joc.3370040103

Nicholson SE (2008) The intensity, location and structure of the tropical rainbelt over west Africa as factors in interannual variability. Int J Climatol 28(13):1775–1785. https://doi.org/10.1002/joc.1507

Nicholson SE (2009) A revised picture of the structure of the "monsoon" and land ITCZ over west Africa. Clim Dyn 32(7–8):1155–1171. https://doi.org/10.1007/s00382-008-0514-3

Nicholson SE (2013) The west African sahel: a review of recent studies on the rainfall regime and its interannual variability. ISRN Meteorology 2013. http://downloads.hindawi.com/journals/isrn.meteorology/2013/453521.pdf

Nicholson SE, Grist JP (2003) The seasonal evolution of the atmospheric circulation over west Africa and equatorial Africa. J Clim 16(7):1013–1030. https://doi.org/10.1175/1520-0442(2003)016

Nicholson SE, Webster PJ (2007) A physical basis for the interannual variability of rainfall in the sahel. Q J R Meteorol Soc 133(629):2065–2084. https://doi.org/10.1002/qj.104

Okumura Y, Xie SP (2004) Interaction of the Atlantic equatorial cold tongue and the African monsoon*. J Clim 17(18):3589–3602

Paeth H, Hall NM, Gaertner MA, Alonso MD, Moumouni S, Polcher J, Ruti PM, Fink AH, Gosset M, Lebel T (2011) Progress in regional downscaling of west African precipitation. Atmos Sci Lett 12(1):75–82

Parker DJ, Thorncroft CD, Burton RR, Diongue-Niang A (2005) Analysis of the African easterly jet, using aircraft observations from the jet 2000 experiment. Q J R Meteorol Soci 131(608):1461–1482

Pascale S, Boos WR, Bordoni S, Delworth TL, Kapnick SB, Murakami H, Vecchi GA, Zhang W (2017) Weakening of the north American monsoon with global warming. Nat Clim Change 7(11):806–812. https://doi.org/10.1038/nclimate3412

Peyrille P, Lafore JP, Redelsperger JL (2007) An idealized two-dimensional framework to study the west African monsoon. Part I: Validation and key controlling factors. J Atmos Sci 64(8):2765–2782. https://doi.org/10.1175/jas3919.1

Pu B, Cook KH (2010) Dynamics of the west African westerly jet. J Clim 23(23):6263–6276

Putman WM, Lin SJ (2007) Finite-volume transport on various cubed-sphere grids. J Comput Phys 227(1):55–78. https://doi.org/10.1016/j.jcp.2007.07.022

Rayner N, Parker DE, Horton E, Folland C, Alexander L, Rowell D, Kent E, Kaplan A (2003) Global analyses of sea surface temperature, sea ice, and night marine air temperature since the late nineteenth century. J Geophys Res Atmos (1984–2012) 108:D14

Redelsperger JL, Diongue A, Diedhiou A, Ceron JP, Diop M, Gueremy JF, Lafore JP (2002) Multi-scale description of a sahelian synoptic weather system representative of the west African monsoon. Q J R Meteorol Soc 128(582):1229–1257

Richter I, Xie SP (2008) On the origin of equatorial Atlantic biases in coupled general circulation models. Clim Dyn 31(5):587–598. https://doi.org/10.1007/s00382-008-0364-z

Roehrig R, Bouniol D, Guichard F, Hourdin F, Redelsperger JL (2013) The present and future of the west African monsoon: a process-oriented assessment of CMIP5 simulations along the amma transect. J Clim 26(17):6471–6505

Shekhar R, Boos WR (2017) Weakening and shifting of the saharan shallow meridional circulation during wet years of the west African monsoon. J Clim 30(18):7399–7422. https://doi.org/10.1175/jcli-d-16-0696.1

Sijikumar S, Roucou P, Fontaine B (2006) Monsoon onset over sudan-sahel: simulation by the regional scale model MM5. Geophys Res Lett 33:3

Siongco AC, Hohenegger C, Stevens B (2015) The Atlantic ITCZ bias in CMIP5 models. Clim Dyn 45(5):1169–1180. https://doi.org/10.1007/s00382-014-2366-3

Skamarock WC, Klemp JB, Duda MG, Fowler LD, Park SH, Ringler TD (2012) A multiscale nonhydrostatic atmospheric model using centroidal voronoi tesselations and c-grid staggering. Mon Weather Rev 140(9):3090–3105

Stocker TF, Dahe Q, Plattner GK (2013) Climate change 2013: The physical science basis. Working group I contribution to the fifth assessment report of the Intergovernmental Panel on Climate Change Summary for Policymakers (IPCC, 2013)

Sultan B, Janicot S (2003) The west African monsoon dynamics. Part II: The preonset and onset of the summer monsoon. J Clim 16(21):3407–3427

Sylla M, Gaye A, Jenkins G, Pal J, Giorgi F (2010) Consistency of projected drought over the sahel with changes in the monsoon circulation and extremes in a regional climate model projections. J Geophys Res Atmos (1984–2012) 115:D16

Thorncroft C, Blackburn M (1999) Maintenance of the African easterly jet. Q J R Meteorol Soc 125(555):763–786. https://doi.org/10.1002/qj.49712555502

Tourre YMV (1981) The squall line over west Africa and tropical eastern Atlantic ocean during gate. PhD Thesis

Vellinga M, Arribas A, Graham R (2013) Seasonal forecasts for regional onset of the west African monsoon. Clim Dyn 40(11–12):3047–3070

Wehner MF, Reed KA, Li F, Bacmeister J, Chen CT, Paciorek C, Gleckler PJ, Sperber KR, Collins WD, Gettelman A et al (2014) The effect of horizontal resolution on simulation quality in the community atmospheric model, CAM5. 1. J Adv Model Earth Syst 6(4):980–997

Willmott C, Matsuura K (2001) Terrestrial air temperature and precipitation: monthly and annual time series (1950–1999) version 1.02. Center for Climatic Research, University of Delaware, Newark

Wu MLC, Reale O, Schubert SD, Suarez MJ, Koster RD, Pegion PJ (2009) African easterly jet: structure and maintenance. J Clim 22(17):4459–4480

Wu W, Lynch AH, Rivers A (2005) Estimating the uncertainty in a regional climate model related to initial and lateral boundary conditions. J Clim 18(7):917–933

Xue Y, De Sales F, Lau WM, Boone A, Feng J, Dirmeyer P, Guo Z, Kim KM, Kitoh A, Kumar V et al (2010) Intercomparison and analyses of the climatology of the west African monsoon in the west African monsoon modeling and evaluation project (WAMME) first model intercomparison experiment. Clim Dyn 35(1):3–27

Zermeno-Diaz DM, Zhang C (2013) Possible root causes of surface westerly biases over the equatorial Atlantic in global climate models. J Clim 26(20):8154–8168. https://doi.org/10.1175/JCLI-D-12-00226.1

Zhai J, Boos WR (2017) The drying tendency of shallow meridional circulations in monsoons. Q J R Meteorol Soc 143(708):2655–2664. https://doi.org/10.1002/qj.3091

Zhang C, Nolan DS, Thorncroft CD, Nguyen H (2008) Shallow meridional circulations in the tropical atmosphere. J Clim 21(14):3453–3470. https://doi.org/10.1175/2007jcli1870.1

Zhao M, Held IM, Lin SJ, Vecchi GA (2009) Simulations of global hurricane climatology, interannual variability, and response to global warming using a 50-km resolution GCM. J Clim 22(24):6653–6678. https://doi.org/10.1175/2009JCLI3049.1